To the Graduate Council:

I am submitting herewith a thesis written by Ronald Earl Goans entitled "A Study of the Release Properties of Sn and SnS from an ISOL-type Target/Ion Source System." I have examined the final electronic copy of this thesis for form and content and recommend that it be accepted in partial fulfillment of the requirements for the degree of Master of Science, with a major in Physics.

Carrol R. Bingham, Major Professor

We have read this thesis
and recommend its acceptance:

Lee L. Riedinger

Jon C. Levin

Accepted for the Council:

Carolyn R. Hodges

Vice Provost and Dean of the Graduate School

(Original signatures are on file with official student records.)

A Study of the Release Properties of Sn and SnS from an ISOL-type Target/Ion Source System

A Thesis Presented for

the Master of Science

Degree

The University of Tennessee, Knoxville

Ronald Earl Goans

May 2011

Copyright © 2011 by Ronald Earl Goans
All Rights Reserved.

Acknowledgements

I would like to thank my advisors, Carrol R. Bingham and H. Kennon Carter, for their tireless devotion to the success of this thesis. I am much indebted to them. I would also like to thank Jon C. Batchelder and Eugene H. Spejewski of UNIRIB, Daniel W. Stracener and Carola Jost of ORNL for their operational assistance and the many useful discussions of RIB development. I acknowledge with much appreciation contributions by Boyce Griffith and Charles Reed in the design stages of this work. I would also like to thank William Peters, Steven Pain, et al. from the experimental nuclear reactions group at the HRIBF and Robert Gryzwacz and Miguel Madurgas of UT for many useful discussions on nuclear structure. Finally, I am enormously appreciative of the HRIBF staff for all of the hard work and long hours they put into the operation of the tandem accelerator. Without their help this thesis would not have been possible.

"When things are going well, something will go wrong. When things just can't get any worse, they will. Anytime things appear to be going better, you have overlooked something." –Richard P. Feynman

Abstract

Radioactive ion beams (RIBs) provide a method for studying the properties of increasingly exotic nuclei. For many nuclei, the intensity of the RIB available in the isotope separation on-line (ISOL) technique is limited by the relatively long delay time in the target/ion source system (TISS). New techniques are needed to decrease this delay time, thereby increasing the intensity of the RIBs available for study.

The sulfide molecular sideband was discovered in 2001 as a way to greatly enhance the quality of Sn beams. Holdup measurements were performed at the Holifield Radioactive Ion Beam Facility (HRIBF) to determine the extent to which the delay of Sn in the TISS is improved by the introduction of sulfur. The results clearly demonstrate that SnS has a shorter delay time than Sn and indicate the improved release efficiency for short half-lives.

The results also indicate that improvements to the formation and release of SnS molecules from the TISS are possible. To this end, modifications were made to the standard HRIBF design to improve the formation and release of molecules from the TISS. The modified TISS design will provide greater control over the TISS parameters by enabling independent and controlled heating of the transfer line and by moving the gas feed line so that it is inserted directly into the target holder. With these improvements, it should be possible to improve the release of Sn isotopes in the sulfide molecular sideband by enabling the formation of the molecule earlier in the release process and by increasing the probability that the molecule will form.

Contents

1 Radioactive Ion Beam Development **1**

1.1 Introduction 1

1.2 ISOL RIB Production 3

1.2.1 Solid State Diffusion 6

1.2.2 Surface Adsorption 7

1.2.3 Ionization 10

1.3 Sn Beams 12

1.3.1 Sulfide Molecular Sideband 12

1.4 Motivation 17

2 Holdup Measurements **19**

2.1 Technique 19

2.2 Experiment 23

2.3 Analysis 27

3 Modified HRIBF-type Target/Ion Source System **33**

3.1 Design 33

3.2 Construction 37

3.3 Characterization 40

4 Conclusions and Implications for Future Research **46**

Bibliography **49**

A Derivation of Yield Measurements **53**

B Adsorption Times **55**

Vita **59**

List of Figures

1.1 Diagram of ISOL RIB production at the Oak Ridge National Laboratory. Image courtesy of the Holifield Radioactive Ion Beam Facility. . 2

1.2 Standard HRIBF target/ion source system with the main components indicated. The target heater is not pictured. 4

1.3 Yields for neutron-rich isotopes measured as Sn and SnS using an EBP ion source. Reproduced with permission from D. Stracener. 14

1.4 Measured ratio of SnS/Sn yields. Reprinted from D.W. Stracener, "Status of radioactive ion beams at the HRIBF," [14], with permission from Elsevier. 14

1.5 Sulfide formation probability as a function of extracted sulfur current, as measured using the FEBIAD-type TISS. Reprinted from R. Kirchner, "Review of ISOL target-ion source systems," [21], with permission from Elsevier. 15

1.6 Profiles of the release of Sn and SnS, measured by Kirchner using the bunched-beam technique. Reprinted from R. Kirchner, "Review of ISOL target-ion source systems," [21], with permission from Elsevier. 15

2.1 Example of a holdup measurement 20

2.2 Layout of the On-Line Test Facility 24

2.3 Graphite target insert. Foil window is 4.5 mg/cm^2 natural molybdenum and catcher material is RVC 'carbon foam'. 25

2.4 Fractional release curves for Sn measured at the target temperatures of 1770 ^{o}C and 1950 ^{o}C. 27
2.5 Fractional release curves of Sn and SnS measured for a target temperature of 1950 ^{o}C 29
2.6 Time constants with associated amplitude coefficients given in parentheses 30
2.7 Efficiencies for finite half-lives calculated from equation 2.11. The quoted efficiency is relative to the system efficiency measured for a stable beam. 32

3.1 Technical drawing of the modified HRIBF-type target/ion source system. Parts labeled are: (a) target heater, (b) target holder, (c) current strap 1, (d) transfer line, (e) cathode, (f) anode chamber, (g) current strap 2 and adaptor, and (h) anode voltage wire 34
3.2 Diagram illustrating the electrical circuit for the modified HRIBF-type TISS. The new transfer line current is indicated with a solid line, whereas the previously existing currents are indicated with dashed lines. 36
3.3 Front view of the modified target/ion source with the main components labelled. 38
3.4 Side view showing the gas line and target insert. 38
3.5 The two points at which the transfer line temperature was measured. 42
3.6 Temperature of the target as determined by measuring the temperature of the graphite insert. 43
3.7 Transfer line temperature as a function of applied current measured at Position 1. The three plots correspond to the three different target temperatures for which the transfer line temperature was measured. . 44
3.8 Transfer line temperature as a function of applied current measured at Position 2. The three plots correspond to the three different target temperatures for which the transfer line temperature was measured. . 44

3.9 Transfer line temperature distributions for a target temperature of 1900 ^{o}C showing the temperatures extrapolated to a transfer line current of 550 A. 45

B.1 Adsorption times for surface temperatures of 1875 ^{o}C and 2050 ^{o}. . . 56

B.2 Adsorption times for surface temperatures of 1875 ^{o}C and 2300 ^{o}. . . 56

B.3 Adsorption times for surface temperatures of 1875 ^{o}C and 1300 ^{o}. . . 57

B.4 Plot of the sticking time (per wall collision) as a function of temperature for Sn and SnS adsorbing to a tantalum surface. The values for the enthalpies of adsorption are taken from [9] and [21]. 58

Chapter 1

Radioactive Ion Beam Development

1.1 Introduction

Knowledge of the atomic nucleus comes from studying it under different experimental conditions. Most of this knowledge relates to nuclei on or near the valley of beta stability. Experiments have shown that nuclear structure changes for nuclei far from stability. The mechanisms by which this occurs are not well understood. To understand this evolution of nuclear structure, new spectroscopic techniques are being developed and implemented. One of these techniques is the use of radioactive ion beams. These radioactive beams have taken on a new importance because they provide a means to study exotic nuclei that were previously inaccessible.

As a subfield of low-energy nuclear physics, radioactive ion beam (RIB) development is concerned primarily with providing high-quality ion beams of radioactive nuclides to experimental end-stations. Here, *high-quality* means both high intensity and high purity. The technical challenges involved in providing high-quality beams of highly unstable nuclides limit the variety of RIBs available for study. New techniques are needed to improve the quality of existing radioactive ion beams.

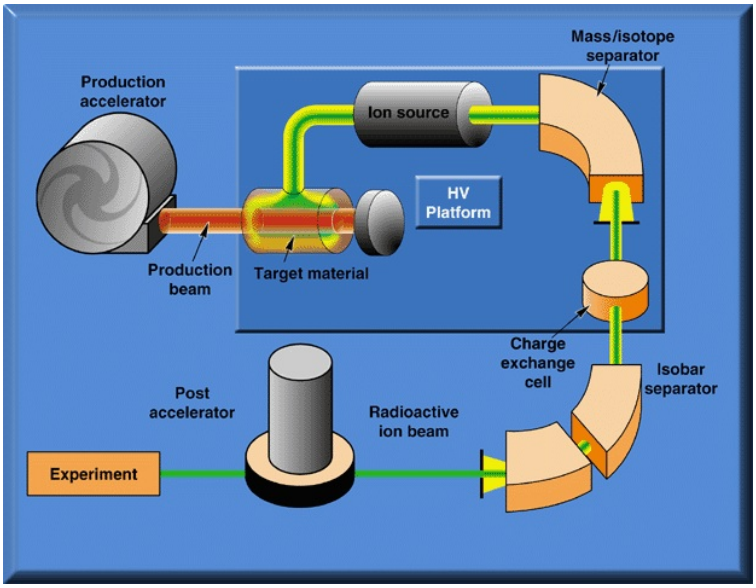

Figure 1.1: Diagram of ISOL RIB production at the Oak Ridge National Laboratory. Image courtesy of the Holifield Radioactive Ion Beam Facility.

The isotope separation on-line technique (ISOL) (illustrated in figure 1.1) is one of two RIB production methods used in radioactive beam facilities around the world. Production of ISOL beams starts inside the target/ion source system (TISS). Figure 1.2 shows an example of a target/ion source system. In this method, a primary beam from the driver accelerator impinges on a target. The primary beam reacts with the target nuclei, inducing the desired nuclear reaction - typically fission, fusion-evaporation, spallation, or fragmentation.

Both thin targets and thick targets are used in ISOL. A thick target is one in which the primary beam is either stopped in the target or exits with an energy below the threshold for inducing the reaction. The reaction products are thermalized within the target itself and must then diffuse out of the target matrix. By contrast, a thin target is one that is sufficiently thin to allow the reaction products to recoil out of the target. Upon exiting the target, the reaction product is thermalized in a catcher. In both cases, the reaction product, often in an ionic state, interacts sufficiently with matter so as to be neutralized. Once the reaction product is released from the target material, it migrates to an ionization region. These ions are extracted and can be

accelerated to an energy appropriate for the particular experiment by using a post-production particle accelerator (typically referred to as the "post-accelerator").

It becomes increasingly important to minimize the isobaric contamination in the beam as research moves to the more exotic nuclei. Isobaric contaminants are isotopes of neighboring elements that are produced in the same reaction, often with production rates several times to several orders of magnitude higher than the nuclide of interest. These contaminants often have masses too close to the mass of the desired nucleus to be effectively removed with traditional electromagnetic separators.

Improving the beam quality consists of a combination of increasing the production rate, effectively separating out the isobaric contamination, and decreasing the delay time in the TISS.

1.2 ISOL RIB Production

The target/ion source system (TISS) is at the heart of radioactive ion beam production in the isotope separation on-line technique. The primary limitation of ISOL-capable RIB production stems from the release properties of an element from the TISS. (An example of a target/ion source system is shown in figure 1.2.) The intensity of the radioactive ion beam that can be delivered to an experimental end-station can be estimated as

$$I_{RIB} = \sigma_{rxn} \cdot N_t \cdot I_{primary} \cdot \epsilon, \tag{1.1}$$

where σ_{rxn} is the reaction cross section, N_t is the number of target atoms per unit area, $I_{primary}$ is the primary beam intensity, and ϵ is a factor necessary to account for losses in beam intensity encountered in the ISOL technique. The beam losses are customarily written in terms of an efficiency, so that ϵ represents the total efficiency for the production and delivery of a RIB. The total efficiency for production and delivery of RIBs is assumed to be a product of the efficiencies for the individual

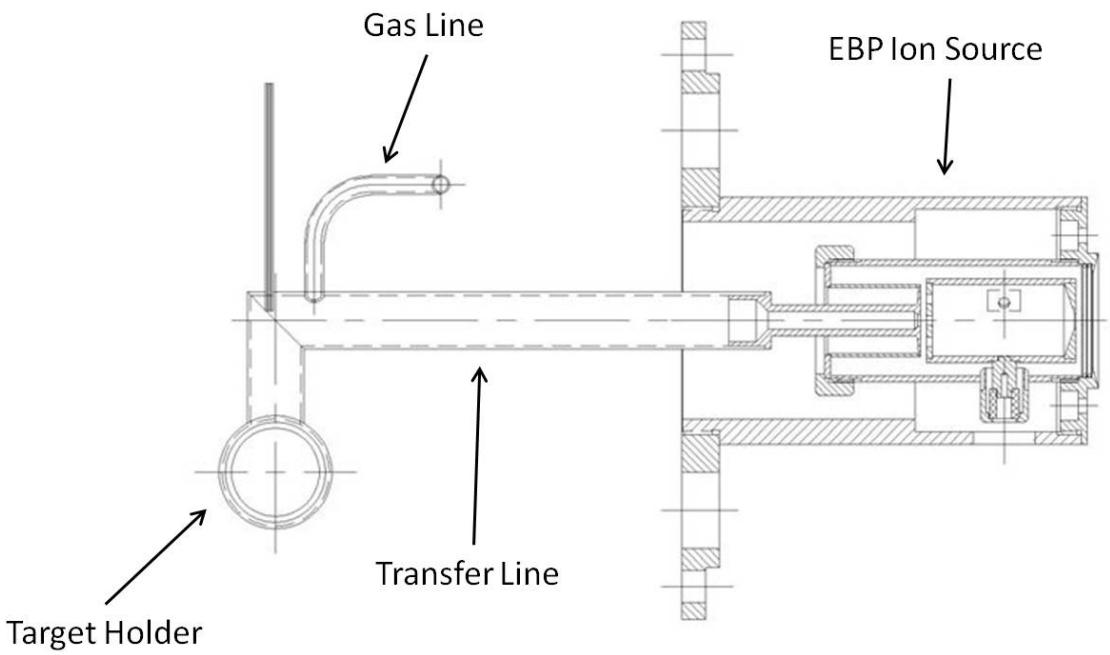

Figure 1.2: Standard HRIBF target/ion source system with the main components indicated. The target heater is not pictured.

processes. Thus, the efficiency is written as

$$\epsilon \equiv \frac{I_{RIB}}{I_{production}} = \epsilon_{TISS} \cdot \epsilon_{ion} \cdot \epsilon_{trans} \cdot \epsilon_{post-accel}, \tag{1.2}$$

where the ϵ's represent the efficiencies for the release from the TISS, ionization, transmission through the beam lines and mass separators, and post-acceleration, respectively. If positive ions are extracted from the TISS, then an additional efficiency is required to account for losses during charge exchange - the process of converting positive ions to negative ions, necessary when the post-accelerator accepts only negative ions.

The ionization efficiency ϵ_{ion} is defined as the ratio of the rate of ions of a particular element extracted from the ion source to the rate of neutral atoms of that element entering the ion source. The ionization efficiency can only be improved by utilizing an ion source that is better suited for ionizing a particular atomic species to the desired charge state. The post-acceleration efficiency refers to the fraction of the radioactive ion beam that can be accelerated to a particular energy and delivered to the end-station. It depends on the type and design of the accelerator used (linac versus Van de Graaff, for example), the desired final beam energy, the charge state stripping efficiency, and transmission through the post-accelerator.

The release efficiency measures the fraction of the reaction products that are able to migrate to the ion source before decaying and, as such, depends on the nuclide's half-life and the delay time inside the TISS. This can be understood in terms of the release time, since the longer a radioactive atom is delayed in the TISS, the less likely it is to be extracted from the TISS before it decays. The release time of a reaction product from the target/ion source system is a complicated and integrated process, resulting from the solid state diffusion time and the surface adsorption/desorption time. One of the primary focuses in ISOL beam development, then, is to minimize the release time from the TISS, often by minimizing these delays individually.

1.2.1 Solid State Diffusion

Reaction products are produced within the bulk of the target matrix. Once produced, the energetic reaction products will be thermalized, either in the target itself (for thick targets) or in the catcher (for thin targets). Once thermalized, the atoms will likely be trapped in interstitial spaces. Qualitatively, the atom must possess an energy sufficient to overcome the potential barrier imposed by the surrounding atoms. Otherwise, the reaction product will not diffuse out of the target matrix before decaying.

Solid state diffusion is described well by the phenomenological relation known as Fick's First Law:

$$\mathbf{J_N} = -D\ \nabla N, \tag{1.3}$$

where J is the flux density of diffusing atoms N and D is the diffusion coefficient. The time-dependent form of equation 1.3 takes the form

$$\frac{\partial N}{\partial t} = D\ \nabla^2 N. \tag{1.4}$$

The diffusion coefficient is known to possess an Arrhenius-like temperature dependence, so that

$$D = D_0 \cdot exp(-\frac{E_A}{k_B T}), \tag{1.5}$$

where E_A is the height of the diffusion barrier, k_B is the Boltzmann constant, and T is the temperature of the bulk material. The barrier height represents the energy a diffusing particle must acquire to move from one interstitial (or lattice) site to the next in a random walk process [1]. Solutions of the one-dimensional diffusion equation have been calculated in an attempt to model the release of reaction products from the target matrix. Solutions have been obtained for the relatively simple geometries of infinite slabs (foil targets), cylinders (fiber targets), and spheres (pressed-powder targets). Fujioka shows in [2] that the fraction f of particles created at time zero

remaining in the bulk at time t is

$$f(\widehat{t}) = \frac{2n}{\pi^2} \sum_{m=1}^{\infty} c_m^{-1} e^{-c_m \widehat{t}}, \tag{1.6}$$

where $\widehat{t}$=($\frac{\pi^2 D}{a^2}$) $\cdot$ t is a characteristic diffusion time. The coefficients c_m and n are given as c_m=(m-$\frac{1}{2}$)^2, ($j_{0,m}/\pi$)^2, and m^2 for foils (n=1), fibers (n=2) and spherical particles (n=3), respectively, and $j_{0,m}$ is the mth positive root of the Bessel function of order zero. The temperature dependence of the diffusion process is given in the diffusion coefficient D (equation 1.5) and indicates that operating at higher target temperatures will increase the fraction of diffusing atoms that are able to overcome the potential barrier and diffuse out of the bulk.

After the atoms have diffused to a surface interface, they must desorb from that surface. The adsorption/desorption process has been studied in much detail. Monte Carlo simulations have shown that atoms will undergo many hundreds, if not thousands, of collisions with the target surfaces before finding the exit aperture. With each collision, the atom will reside on the surface for an average amount of time given by the phenomenological relationship known as the Frenkel equation (discussed below).

1.2.2 Surface Adsorption

Migration of reaction products out of the target holder and through the transfer line occurs through effusion. The pressures inside the target holder and transfer line are taken to be sufficiently small so that the effusion is carried out in the molecular flow regime. The molecular flow regime exists when the mean free path is much greater than some characteristic length scale. For long tubes of inner diameter D, molecular flow is achieved for λ>>D, where D is typically a few centimeters or less for target/ion source systems. For particles with a mean energy $\sim k_B T$ inside a container held at high vacuum ($\sim 10^{-6}$ torr), the mean free path is on the order of 10 meters.

Thus, the condition for molecular flow is easily satisfied. Physically, this implies that effusing particles undergo far more particle-wall collisions than they do particle-particle collisions. Effusive flow is determined primarily by the particle-wall collisions [3].

The delay time introduced by the effusion process is determined largely by the time for a single adsorption-desorption cycle to occur. In this process, particles will adsorb to a wall surface and will stay adsorbed to the wall for an average amount of time known as the adsorption time (also referred to as the residence or sticking time). The adsorption time describes the mean time the particle remains in a potential well of height E_{ads} before acquiring an amount of energy from lattice vibrations sufficient to escape the adsorption potential [4]. Phenomenologically, the sticking time per wall collision, t_s, of a particle on a surface maintained at a temperature T is described by the Frenkel equation, so that

$$t_s = t_0 \cdot exp(\frac{\Delta H_{ads}}{k_B T}), \tag{1.7}$$

where t_0 is the inverse of the Debye frequency, ΔH_{ads} is the enthalpy of adsorption for the particular adsorbent/adsorbate combination, and $k_B T$ has the usual meaning. The Debye frequency is

$$\nu_D = v_s \cdot (\frac{3}{4\pi}\frac{N}{V})^{1/3}, \tag{1.8}$$

where v_s is the velocity of sound in the material and $\frac{N}{V}$ is the corresponding particle number density [1]. In the Debye model for phonons, the Debye frequency is taken as an upper limit for the allowed phonon frequencies. The constant t_0 takes the form

$$t_0 = \frac{1}{\nu_D} = \frac{1}{v_s}(\frac{4\pi}{3}\frac{V}{N})^{1/3}. \tag{1.9}$$

If ν_D represents the maximum frequency of lattice vibrations, then t_0 is taken as the minimum time a particle can reside on a surface. There are discrepancies in the literature regarding the appropriate value of t_0 for tantalum. Some authors contend

that $t_0 \sim 10^{-13}$ seconds, whereas others give $t_0 \sim 10^{-15}$ seconds. Since much of this work is based on results obtained by R. Kirchner, his value of $t_0 = 2.4 \cdot 10^{-15}$ seconds will be adopted here.

As no pressure gradient exists in the molecular flow regime, the direction of motion is determined by the direction in which an effusing particle releases from a surface. This direction is determined by the so-called Knudsen cosine law [5], which states simply that the number of particles dN releasing from the surface in a solid angle $d\Omega$ is proportional to the cosine of the angle θ relative to the normal of the surface, so that

$$dN = \frac{n}{\pi} cos(\theta) d\Omega, \tag{1.10}$$

where n is the normal to the surface. It can be seen immediately that equation 1.10 is azimuthally symmetric. This azimuthal symmetry indicates that a particle is equally as likely to go forward as it is to go backward when it releases from a surface. Equation 1.10 implies that a particle will likely undergo many collisions with the wall surfaces, bouncing around in many different directions, before effusing through the exit aperture.

With the surface residence time in mind, the target, the target holder, and the transfer line can be thought of as the sources of an additional delay time. This delay time, referred to as the effusion time $t_{effusion}$, can be written as the sum of the in-target effusion and the effusion through the transfer line. Thus,

$$\begin{aligned} t_{effusion} = t_{eff}^{target} + t_{eff}^{holder} + t_{eff}^{TL} = [n_{coll} \cdot (t_{flight} + t_s)]_{target} + \\ + [n'_{coll} \cdot (t'_{flight} + t'_s)]_{holder} + [n''_{coll} \cdot (t''_{flight} + t''_s)]_{TL}, \end{aligned} \tag{1.11}$$

where n_{coll} is the number of wall collisions made by the effusing particle, t_s is the sticking time, t_{flight} is the flight time between wall collisions, and the subscripts 'target', 'holder' and 'TL' indicate the effusion processes out of the target, the target container and through the transfer line. Equation 1.11 indicates that the *total* effusion

time depends on the effusion of particles from the target matrix, the target holder, and through the transfer line.

The release time of a particle from the TISS can now be written as

$$t_{release} = t_{diff} + t_{effusion} = t_{diff} + [n_{coll} \cdot (t_{flight} + t_s)]_{target} + \\ +[n'_{coll} \cdot (t'_{flight} + t'_s)]_{holder} + [n''_{coll} \cdot (t''_{flight} + t''_s)]_{TL}, \quad (1.12)$$

where t_{diff} represents the solid state diffusion time, i.e., the time for a particle to diffuse to a target surface.

1.2.3 Ionization

The primary type of ion source in use at the HRIBF is the Electron Beam Plasma (EBP) ion source. Plasma ion sources are not selective because they are capable of ionizing a wide range of elements and molecules. The EBP ion source utilizes the electron-impact ionization technique. In electron-impact ionization, neutral atoms are converted to positive ions by way of electron-atom collisions, so that the (e,(n+1)e) ionization reaction takes the form

$$e + X \rightarrow X^{n+} + (n+1)e. \quad (1.13)$$

The likelihood of ionizing an atom to a charge state q=n+ depends on the ionization potential of the desired charge state, $\Phi_{0\rightarrow n+}$, and the bombarding electron energy E_e. It has been determined experimentally that the ionization cross section varies from zero for electron energies just below the ionization potential to a maximum for electron energies about 3-4 times the desired ionization potential [6].

In the HRIBF EBP ion source, the primary electrons are produced by thermionic emission from the cathode and are accelerated into the anode chamber. The incident electron energy is determined by maintaining the anode chamber at a positive voltage

relative to the cathode. Thermionic emission is described well by the Richardson-Dushman Equation:

$$J = A \cdot b \cdot T^2 \cdot exp(\frac{-eW}{k_B T}), \tag{1.14}$$

where J is the current density (in units of Acm^{-2}), A is a universal constant equal to 120.4 A cm^{-2}K^{-2}, b is a unitless material-dependent correction factor, W is the material's work function, and T and k_B have the usual meanings. For tantalum, W=4.12 V and A $\cdot b = 60 Acm^{-2}$K^{-2} [6].

To provide the temperatures necessary for thermionic emission, the cathode is heated resistively by driving several hundred amps of current through the cathode, which is designed to have a high electrical resistance. The cathode current is typically maintained between 340-360 A and is adjusted as needed to maintain an anode current between 150-160 mA. The anode current measures the drain on the anode voltage supply and is determined primarily by the primary electron current entering the anode chamber. For the HRIBF system, the ionization efficiency was measured to be relatively constant for electron energies between 120 eV and 180 eV. Given this range, an energy of 150 eV was chosen as the standard energy to optimize the formation of 1+ ions for a broad range of elements.

A set of three solenoid magnets surrounds the ion source chamber to improve the efficiency of the EBP ion source. They provide magnetic confinement of the plasma and the electron current within the anode chamber. In addition, varying the magnetic field inside the anode changes the plasma density, which can be adjusted to increase the density of ions in the extraction region. Thus, the magnetic field produced by the solenoid magnets can be adjusted to optimize the release of ions extracted from the ion source.

1.3 Sn Beams

The closed-proton shell element Sn has long been a subject of ISOL beam development. With its magic number of protons, Sn isotopes (including the magic N=50 and N=82) provide an ideal laboratory for studying the evolution of nuclear structure across a wide range of neutrons. (See [7], [8], and the references therein for discussions of the nuclear physics of Sn isotopes.)

Providing high-quality beams of short-lived Sn isotopes has proven challenging in ISOL. The adsorption enthalpy for Sn on a tantalum surface was determined to be 4.5 eV [9]. The temperature dependence of the mean sticking time, shown in equation 1.7, indicates that surface temperatures below about 1800 K give prohibitively long residence times. Accordingly, losses inside the target/ion source can only be minimized by running the TISS at very high temperatures, by changing either the adsorbing particle or the surface to which it adsorbs, or by a combination of the two. Physical requirements of target/ion source systems limit the materials that can be used. This implies the necessity of changing the form of the Sn isotopes being released from the TISS, which can be achieved through the molecular sideband method.

1.3.1 Sulfide Molecular Sideband

The molecular-sideband technique has been used extensively in ISOL. The method requires introducing vapors of a molecule-creating substance so that an appropriate molecule can be formed from the reaction product and the vapors. An appropriate molecule is one in which the molecular form is less reactive with the surfaces of the target/ion source system and will thus have a shorter delay in the system. Additionally, extracting and mass separating at the molecular-ion mass can reduce the isobaric contamination. (See, for example, [10], [11], [12], and [13] for further discussions of the molecular-sideband technique and its use in ISOL systems.)

A prime example of the molecular-sideband technique was demonstrated in 2001 when D. Stracener announced in a world-wide web release the discovery of radioactive

Sn isotopes extracted and mass-separated as $^{A}\mathrm{Sn}^{32}S^{+}$ [14]. The experiment was performed to measure the yields of fission fragments from an open matrix uranium carbide target. However, the TISS used was contaminated with sulfur from a previous experiment. Measurements of the yields of the neutron-rich Sn isotopes produced in the 40 MeV proton-induced fission of ^{238}U showed the ratio of $\frac{SnS^{+}}{Sn^{+}}$ increased for decreasing half-life (figures 1.3 and 1.4). (See Appendix A for a derivation and explanation of yield measurements.) Stracener's conclusion was that SnS migrated through the TISS with a shorter delay time than atomic Sn. This smaller delay time would allow a larger fraction of short-lived SnS to migrate through TISS before decaying. Stracener discovered that extracting as SnS^{+} showed a significant reduction in the contaminating isobars, because the neighboring isobars either do not form stable sulfide molecules under these conditions or, more likely, they do not form stable molecular ions. Regardless, reduction of the isobaric contamination allows for providing beams of essentially pure Sn.

News of this discovery spurred R. Kirchner at GSI-Darmstadt to investigate in detail the release properties of SnS for the FEBIAD-type target/ion source system in use at that facility. Kirchner's results (summarized in figures 1.5-1.6) were obtained in a series of off-line measurements.

In his studies, Kirchner introduced sulfur into the TISS in a controlled way by using a variable leak valve to determine the threshold for maximizing the formation probability. Figure 1.5 shows that the formation probability, $\beta=\frac{SnS^{+}}{Sn^{+}+SnS^{+}}$, saturates for measured sulfur currents near 1 μA - low enough to avoid suppressing the ion source efficiency. The extracted sulfur current is proportional to the flow rate of sulfur inside the TISS. The flow rate of sulfur atoms inside the TISS determines the surface coverage, and the coverage of sulfur atoms on the surface determines the formation of SnS.

Physically, this is reasonable. Since the likelihood of in-flight collisions is small, Sn is likely to react with and form the sulfide molecule while it resides on the surface. The likelihood of in-flight collisions is extremely small. Increasing the concentration

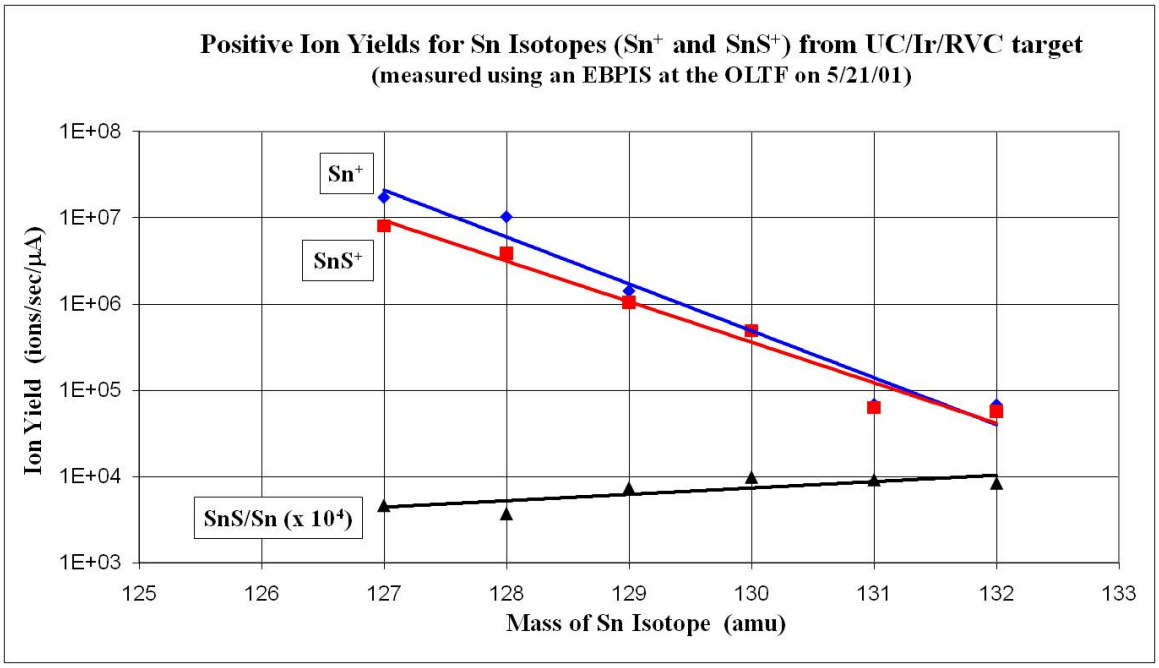

Figure 1.3: Yields for neutron-rich isotopes measured as Sn and SnS using an EBP ion source. Reproduced with permission from D. Stracener.

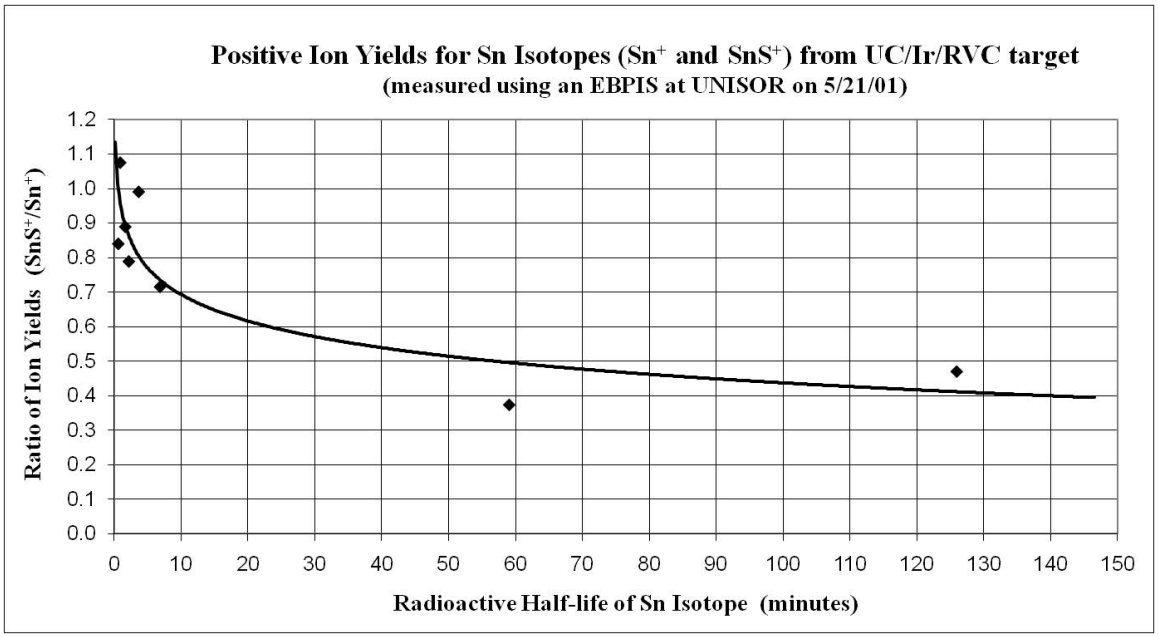

Figure 1.4: Measured ratio of SnS/Sn yields. Reprinted from D.W. Stracener, "Status of radioactive ion beams at the HRIBF," [14], with permission from Elsevier.

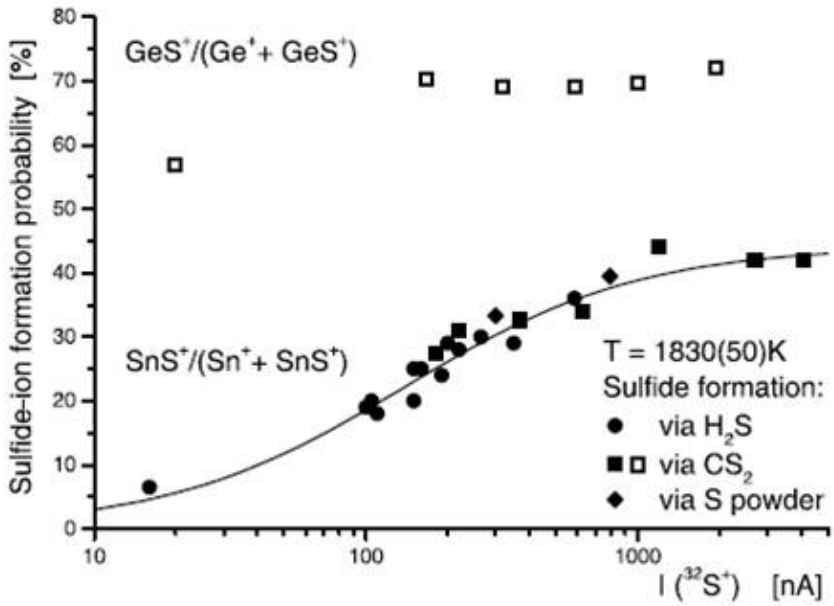

Figure 1.5: Sulfide formation probability as a function of extracted sulfur current, as measured using the FEBIAD-type TISS. Reprinted from R. Kirchner, "Review of ISOL target-ion source systems," [21], with permission from Elsevier.

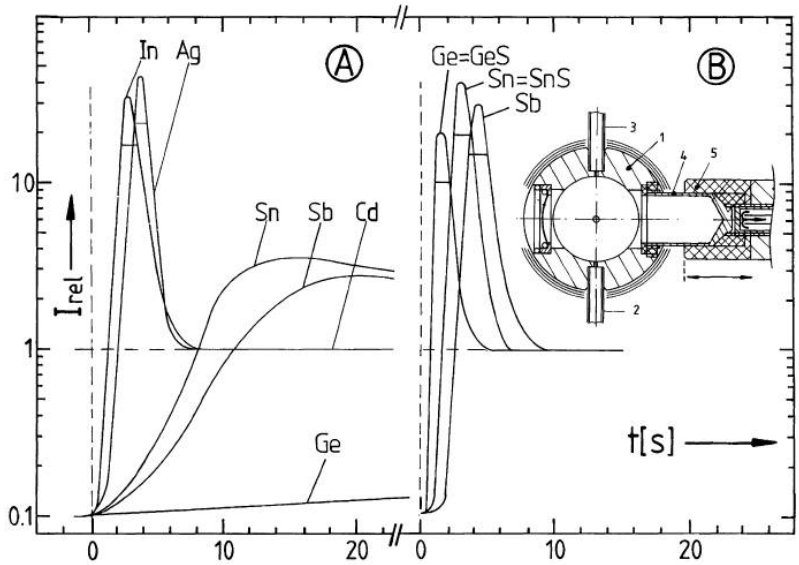

Figure 1.6: Profiles of the release of Sn and SnS, measured by Kirchner using the bunched-beam technique. Reprinted from R. Kirchner, "Review of ISOL target-ion source systems," [21], with permission from Elsevier.

of sulfur atoms on the surfaces of the TISS should increase the likelihood that a Sn atom will react with a sulfur atom to form SnS. The amount of SnS that is able to form will reach a maximum for some value of sulfur. Thus, it remains to determine the minimum value of sulfur needed inside the TISS to maximize the formation of SnS. Furthermore, the SnS formation probability depends on the surface residence time. Qualitatively, the shorter the residence time, the less likely it is for a Sn atom to react with a sulfur atom to form the sulfide molecule. By assuming exponential dependences, Kirchner derived a relationship for the formation probability, β, as a function of the ratio $\frac{t_f}{t_s}$, where t_f is the mean formation time, so that

$$\beta = \beta_{sat} \int_0^\infty \frac{1}{t_f} e^{-\frac{t}{t_f}} e^{-\frac{t}{t_s}} dt = \beta_{sat} \cdot \frac{t_s}{t_s + t_f} = \beta_{sat} \cdot \frac{1}{1 + \frac{t_f}{t_s}}. \tag{1.15}$$

Equation 1.15 implies that the likelihood of forming SnS depends on the concentration of sulfur inside the TISS and on the mean residence time for Sn. Conceptually, both conclusions are reasonable.

Kirchner also conducted a set of bunched-beam experiments to measure the mean sticking times for Sn and SnS. In the bunched-beam experiment, a cooling block was applied to the TISS, creating a cold trap. The cooling block forces the less volatile test vapors to condense and accumulate in the cold trap. Quick removal of the cooling block allows the TISS to heat up rapidly, allowing the test vapors to migrate through the system. The extracted current is then measured, enabling determination of the release profiles. Kirchner has used this method in conjunction with computer simulations [9] to determine the average residence time of an atom on the TISS surface.

Figure 1.6 shows the results of the off-line bunched-beam measurements for Sn and SnS. The left plot gives the measured release profiles before sulfur was introduced, and the right plot shows the release profiles after sulfur was introduced. Plotted here are the intensities of the release profiles relative to the current measured without the cooling block applied. The insert in the right plot shows the FEBIAD TISS

with cooling block that was used for the bunched-beam experiments. The results show that Sn has a mean sticking time of approximately 6 ms on Ta at 1830 K. Under identical operating conditions and with the sulfur concentration already in saturation, the mean sticking time for SnS was determined to be on the order of μs. This indicates a substantial improvement in the mean sticking time for SnS. The bunched-beam experiments also showed essentially identical release profiles for Sn and SnS after sulfur was introduced. Kirchner concluded that the identical release profiles result from complete conversion of Sn to SnS. To determine the extent to which the neighboring isobars form stable sulfide ions, Kirchner introduced tracer vapors of primarily Ag, In, Cd, and Sb. The absence of measureable currents of the contaminant tracers yielded upper limits on the ratio of the tracer sulfide to the tracer element on the order of 10^{-4} [15].

1.4 Motivation

Since the discovery of the tin sulfide sideband, the Holifield Radioactive Ion Beam Facility routinely uses the technique for production and delivery of pure beams of Sn for nuclear physics experiments. For the on-line production of neutron-rich Sn isotopes, the HRIBF floods the TISS with an amount of sulfur sufficient to suppress the ion source efficiency and then continues to flood the system for several hours. The sulfur introduction is then stopped, the ion source efficiency recovers relatively quickly, and the proton beam is put on target. In this way, the HRIBF is able to provide pure beams of neutron-rich Sn isotopes for about two weeks before the process needs to be repeated. This method does not afford control over, or optimization of, the sulfide chemistry.

Detailed studies have not yet been carried out with the HRIBF target/ion source system to determine the minimum conditions for optimizing the release of SnS. Kirchner's results, though, strongly indicate the possibility of improving the formation and release of SnS from the HRIBF target/ion source system. Direct measurements of

the release properties of SnS from the HRIBF target/ion source system are needed. It is believed that controlling the introduction of sulfur into the TISS will determine the minimum sulfur concentration necessary to maximize the sulfide formation, thereby preventing a decline in the ionization efficiency. Fully investigating the release properties of Sn and SnS will requires a target/ion source system with variable temperature distribution and control over the introduction of molecule-forming gases.

Chapter 2

Holdup Measurements

2.1 Technique

The delay of a particle in the target/ion source system can be determined through a type of experiment referred to as a holdup measurement. This type of experiment gives a direct measurement of the delay time in the TISS and the overall TISS efficiency for a species by measuring the change in the rate of particles exiting the TISS as a function of time.

When available, a heavy-ion beam of a stable isotope, and of sufficiently high intensity, is used to measure the holdup time in the system. Using a heavy-ion beam to perform holdup measurements reduces the measurement time interval to the sub-second level, thereby improving the accuracy of the measurement. Additionally, holdup measurements performed with a stable beam provide extracted beam intensities up to several orders of magnitude greater than those provided by holdup measurements using radioactive beams. The increased beam intensities enable the use of a Faraday Cup connected to a data plotter to measure the extracted current.

To perform the holdup measurement with a heavy ion beam, the primary beam is turned on and the extracted current is measured as it builds up to a saturation value.

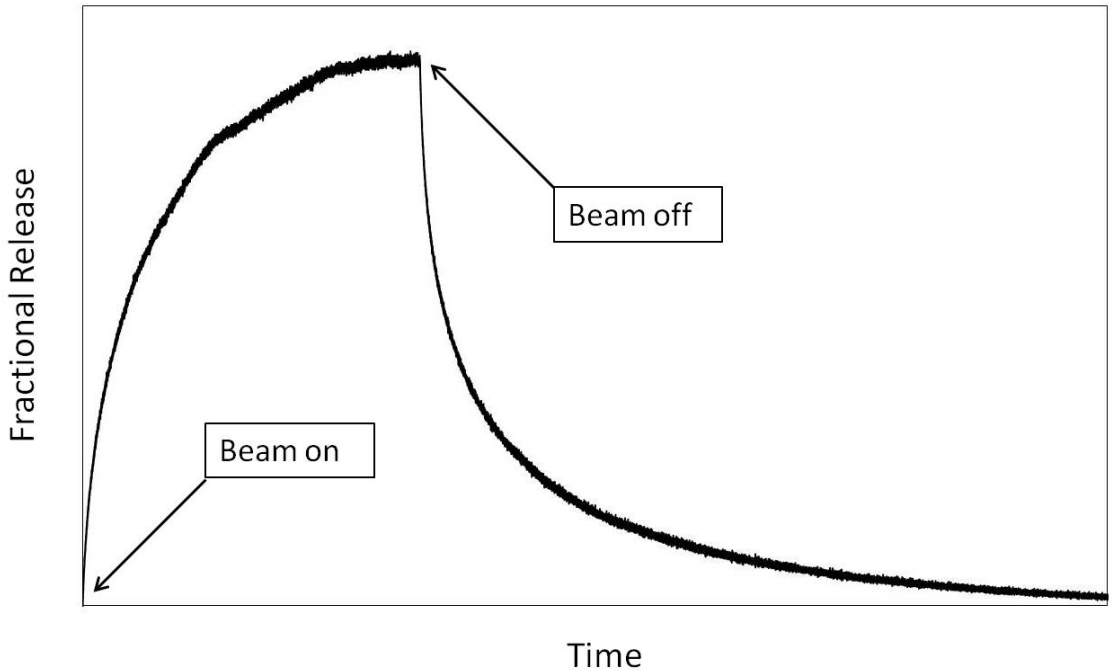

Figure 2.1: Example of a holdup measurement

Once it has been determined that equilibrium has been established, the primary beam is turned off and the current is measured as the extracted beam falls back to zero.

An example of a typical holdup measurement is illustrated in figure 2.1. The holdup measurement can be considered in two parts: the build-up (or beam on) measurement and the decay (or beam off) measurement. One important aspect is noticed immediately from figure 2.1. The time required to build up to equilibrium is shorter than the time for the equilibrium concentration to drop to zero when the beam is turned off. This difference is believed to be a result of localized heating from the heavy ion beam, since the diffusion and adsorption/desorption processes are sensitive to the temperature of the material.

The absolute TISS efficiency for an element can be determined by measuring the ratio of the mass-separated beam to the production rate after equilibrium has been established. For stable beam experiments, where the energy of the primary beam is below the threshold to induce a nuclear reaction, the production rate is equal to the

intensity of the primary beam. Thus,

$$\epsilon_{TISS} = \frac{I_{sat}}{\epsilon_t I_{primary}}, \tag{2.1}$$

where ϵ_t is the transmission efficiency of the mass separator and is believed to be about 80% for the dipole magnet used at the On-Line Test Facility. For a beam of stable atoms, the TISS efficiency ϵ_{TISS} is approximately equal to the ion source efficiency for that element. The value for I_{sat} is determined by taking an average over a large number of data points before the beam is turned off so as to minimize the statistical uncertainty in I_{sat}.

Qualitative assessments of the delay time can be made by comparing plots of the fractional release F(t). The fractional release is taken as the ratio of the measured current to the saturation value. Normalizing the data sets in this way allows for direct, side-by-side comparisons of the delay in the TISS. Fractional release curves give a qualitative indication of the delay time by showing how quickly a particular beam builds up to its equilibrium value. Since the normalization ensures that $F(t=\infty)=1$, fractional release curves do not provide any information on the absolute beam intensity or the TISS efficiency.

A common figure of merit used in describing release measurements is the 50% time t_{50}, which describes the time it takes for the measured current to reach half of its maximum value. The t_{50} time is determined directly from the data by averaging over all of the data points in the interval $\frac{1}{2}I_{sat} \pm \delta\ I_{sat}$, where δI_{sat} is the propagated error of the saturation current resulting from the scatter in the data.

R. Kirchner describes in [15] a purely phenomenological approach for determining the release profile of an element from a TISS. Kirchner used a bunched-beam technique, whereby vapors of the element are accumulated in a cold trap. At time zero, the cooling block is removed so the cold trap heats up swiftly. Quick removal of the cold block effectively releases all of the test vapors at time zero. Kirchner's approach was to assume that the current at time t is proportional to the probability

for a particle to be released from the TISS. Thus, the fractional release is described by

$$F(t) = \frac{I(t)}{I_{sat}} = \int_0^t p(t')dt', \tag{2.2}$$

where p(t') is the release function. Hence, the integral describes the probability that a particle created at time zero will be released at time t. This equation is only valid for pulsed beams and Kirchner's bunched beam experiments. However, the formalism can be adapted for experiments where the production rate is continuous, not pulsed. The measured fractional release then becomes

$$F(t) = \frac{I(t)}{I_{sat}} = \int_0^t p(t-t')dt'. \tag{2.3}$$

The integral now represents the probability that a particle created at time t' will be released at time t. The release function p(t) can be derived from the experimentally measured fractional release in the usual way:

$$\frac{dF}{dt} = \frac{d}{dt}\int_0^t p(t-t')dt' = p(t). \tag{2.4}$$

Knowledge of the release function p(t) allows for the calculation of the reduction of the efficiency due to radioactive decay inside the TISS. To see this, the half-life dependence of the efficiency can be written as

$$\epsilon(t_{\frac{1}{2}}) = \int_0^\infty p(t')exp(-\frac{ln2}{t_{\frac{1}{2}}}t')dt'. \tag{2.5}$$

Physically, the half-life dependence of the efficiency represents the likelihood that a particle created at time t' will be released from the TISS and will not have decayed. Thus, the half-life dependence of the efficiency can be thought of as resulting from the overall delay inside the TISS. It should be noted that $\epsilon(t_{\frac{1}{2}})$ calculated in this way is a *relative* efficiency, where $\epsilon(t_{\frac{1}{2}})$=1 corresponds to the relative efficiency for a stable

beam. The absolute system efficiency as a function of half-life can be calculated by multiplying $\epsilon(t_{\frac{1}{2}})$ by the stable beam efficiency ϵ_{system}.

A final quantity commonly used to compare release profiles is the average release time and can be calculated once p(t) is determined. The average release time is simply the mean time of the fractional release curve and is calculated as

$$< t_{release} >= \frac{\int_0^\infty tp(t)dt}{\int_0^\infty p(t)dt}. \tag{2.6}$$

Unlike the 50% time, the average release time represents a global average over the entire beam-on (or beam-off) curve. As such, it will be weighted heavily by the long time component of the release function. However, for shorter release times, weighting by the long time component will be less influential.

The utility of holdup measurements stems from their ability to predict the yield of a radionuclide. Since holdup experiments directly measure the release of an atom (or molecule) from the TISS and do not rely on theoretical calculations of the release properties, the possible RIB intensity can be calculated in a simple and reliable way. The holdup measurement allows for the determination of $\epsilon(t_{\frac{1}{2}})$, which in turn allows for the yield Y to be calculated for a particular nuclide as

$$Y = R \cdot \epsilon = I_{primary} \cdot \sigma_{rxn} \cdot N_t \cdot \epsilon(t_{\frac{1}{2}}) \cdot \epsilon_{system}. \tag{2.7}$$

The yield as calculated here corresponds to the rate of ions/sec of a nuclide produced in a particular reaction and extracted from the TISS after the system has reached equilibrium.

2.2 Experiment

Holdup measurements were performed at the On-Line Test Facility (OLTF) (figure 2.2) located in the Holifield Radioactive Ion Beam Facility at the Oak Ridge National

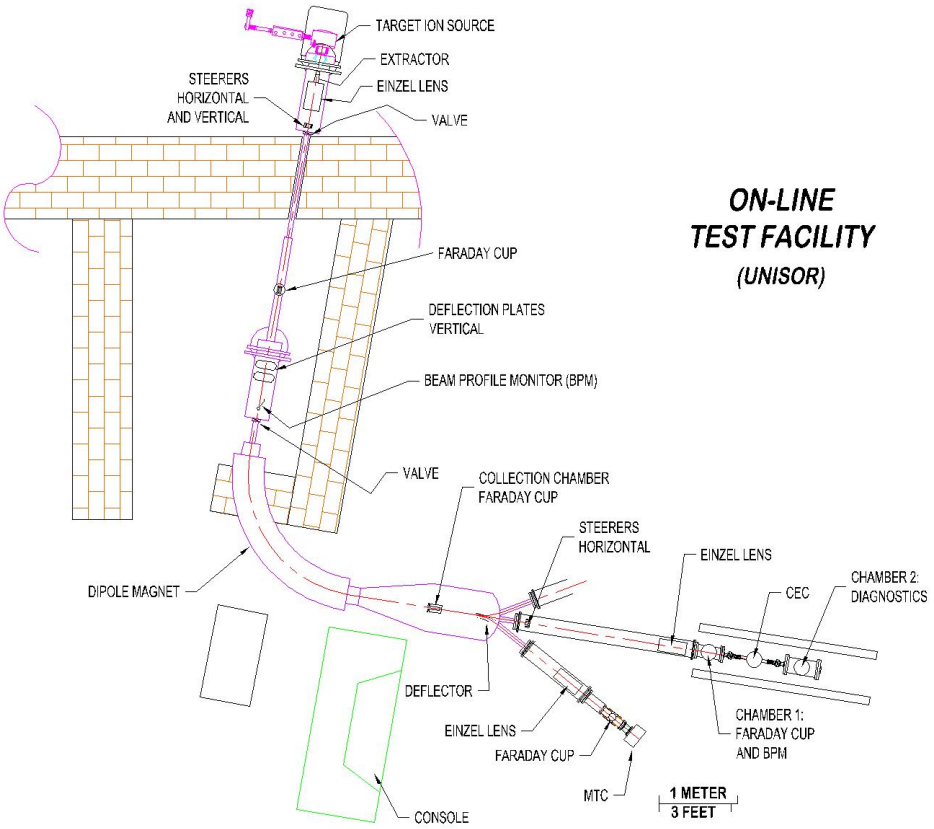

Figure 2.2: Layout of the On-Line Test Facility

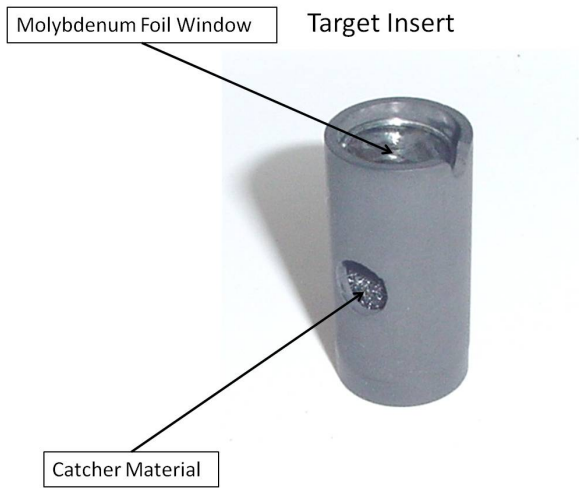

Figure 2.3: Graphite target insert. Foil window is 4.5 mg/cm^2 natural molybdenum and catcher material is RVC 'carbon foam'.

Laboratory. The target/ion source systems used and tested at the OLTF take beams directly from the tandem accelerator, a folded 25 MV Van de Graaff particle accelerator. The extraction region of the TISS connects into the OLTF beam line. For mass separation, the OLTF utilizes a 90° dipole magnet with a separation resolution $\frac{m}{\Delta m}$=2,000. This is sufficient for isotopic separation but not isobaric separation. For these measurements, the mass-separated current was measured on the Faraday Cup before the beam line split, labeled 'Collection Chamber Faraday Cup' in figure 2.2.

To measure the release profile of Sn and SnS from the standard HRIBF target/ion source system, a heavy-ion beam of ^{120}Sn was incident on the target insert, an example of which is pictured in Figure 2.3. The insert was made of a high-purity graphite and contained a thin foil window to degrade, but not stop, the beam. The catcher was a 2-cm thick slice made from an open graphite matrix that had been previously shown in unpublished holdup measurements [16] to possess good release properties. This carbon 'foam' was produced by Babcock and Wilcox using a reticulated vitreous carbon (RVC) matrix [17]. The RVC matrix has an open fiber structure, with fiber diameters around 60 μm and a surface area of 23.8 cm^2/cm^3.

For these measurements, approximately 20 particle nA of 140 MeV $^{120}Sn^{8+}$ was incident on the target holder. Due to the relatively short range of heavy ions in matter (on the order of a few microns for 140 MeV ^{120}Sn in carbon), the standard graphite window of the target insert was replaced by a thin window of 4.5 mg/cm^2 natural molybdenum. The Stopping and Ranges of Ions in Matter (SRIM) program [18] was used to calculate the total loss of beam energy for ^{120}Sn in natural molybdenum, as well as the implantation depth of the degraded Sn beam in the catcher. The calculations showed that the initial 140 MeV ^{120}Sn loses approximately 132 MeV passing through the thin foil window and, thus, enters the catcher material with an energy of about 8 MeV. At this energy, the implantation depth is about 2.65 μm for ^{120}Sn in carbon.

The data were acquired using a Faraday Cup connected to a modified Keithley model 26000 0-10 V Logarithmic picoAmmeter, whose circuit was modified in-house by J. Blankenship. The voltage output from the picoammeter was collected and plotted using WinDAQ's DATAQ model DI-718B-ES data logger.

The TISS is equipped with fixed leaks of krypton and xenon to monitor the efficiency of the ion source. The krypton and xenon fixed leaks are calibrated to have leak rates of $4.0{\cdot}10^{-7}$ atm·cc/s and $2.4{\cdot}10^{-7}$ atm·cc/s at 23 ^{o}C. One atm·cc/s corresponds to approximately $2.62{\cdot}10^{19}$ particles per second, so that the fixed leak rates are about $1.0{\cdot}10^{13}$ pps for krypton and $9.0{\cdot}10^{12}$ pps for xenon. ^{84}Kr has a natural isotopic abundance of 57.00% and ^{132}Xe has a natural isotopic abundance of 26.91% [19]. Accounting for these, the flow rates of ^{84}Kr and ^{132}Xe are determined to be $5.7{\cdot}10^{12}$ pps and $2.4{\cdot}10^{12}$ pps, respectively.

Before the holdup measurements were started, background currents were measured for masses 32, 34, 84, 132, 120 and 152 (corresponding to ^{32}S, ^{34}S, ^{84}Kr, ^{132}Xe, ^{120}Sn and ^{120}Sn^{32}S). An insignificant current of 2.4 nA was measured for ^{32}S, confirmed by the measured current at mass 34 and the isotopic ratio of ^{34}S/^{32}S. The small sulfur contamination is likely a result of sulfur impurities in the materials used in the construction of the target/ion source system. The ^{84}Kr and ^{132}Xe currents

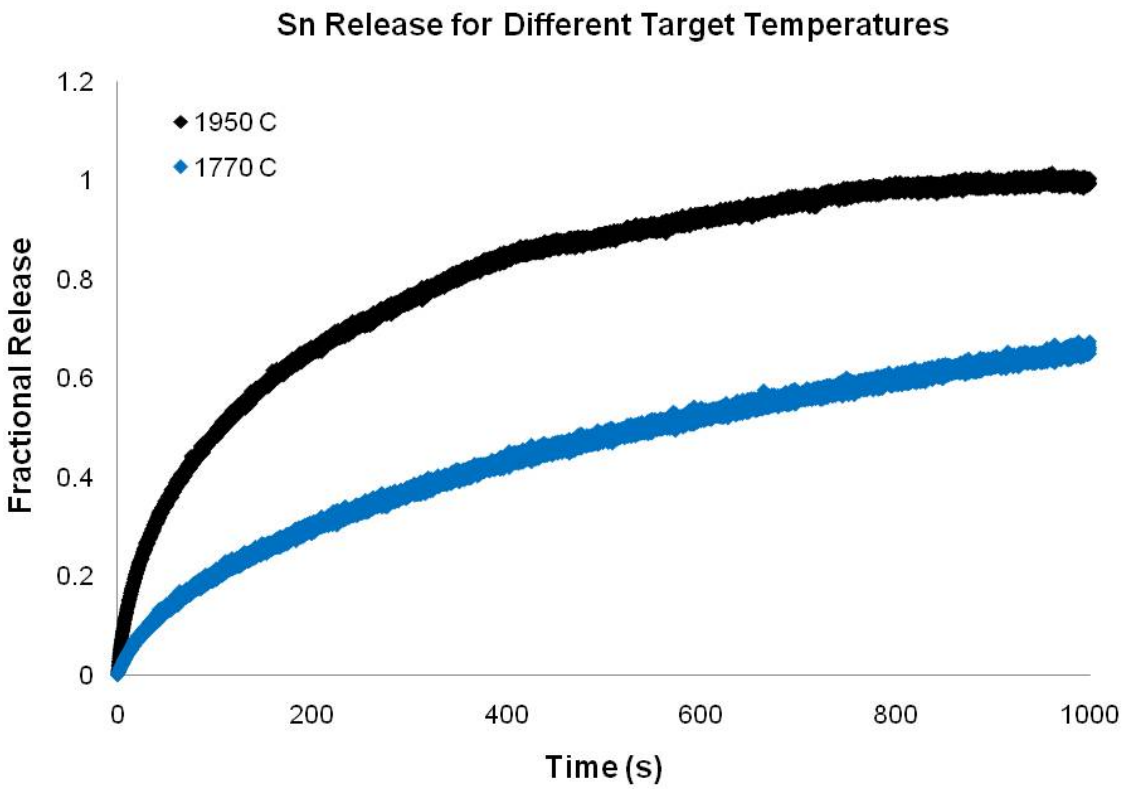

Figure 2.4: Fractional release curves for Sn measured at the target temperatures of 1770 ^{o}C and 1950 ^{o}C.

were initially measured to be 53.5 nA and 28.2 nA, respectively, and were measured throughout the experiment to monitor the efficiency of the ion source.

2.3 Analysis

The release profile of Sn was measured for target temperatures of 1770 ^{o}C and 1950 ^{o}C. For both target temperatures, the primary beam current was between 20 and 22 particle nA, eliminating effects from differences in beam heating. The fractional release curves in figure 2.4 clearly indicate that the release of Sn has a strong dependence on the target temperature. The t_{50} time for 1770 ^{o}C was determined to be 553 $\pm$ 50 seconds. The 50% time decreased to 108 $\pm$ 10 seconds for a target temperature of 1950 ^{o}C. This can be understood in terms of the temperature

dependence for both the bulk diffusion of Sn atoms from the graphite matrix and the adsorption time of Sn on carbon surfaces during the effusion of Sn from the target container.

After the no-sulfur baseline measurements were collected, sulfur was introduced into the system by feeding H_2S gas through a Granville-Phillips Series 203 variable leak valve. The variable leak valve is designed to allow controlled introduction of gases into the system. Unfortunately, due to an unexpected failure of the gas line, only a single holdup measurement for SnS at the highest target temperature (1950 ^{o}C) was obtained. The intensity of the primary beam was 21 particle nA and the ion current for ^{32}S, which is assumed to be proportional to the concentration of sulfur within the TISS, was measured to be about 100 nA. It is believed that this measurement, though not taken under ideal conditions, is at least representative of the release properties of SnS. Furthermore, this sulfur concentration is closer to those measured during RIB production at the HRIBF than what Kirchner found to optimize the SnS formation [20, 21].

Comparing the fractional release curves in figure 2.5 clearly shows that SnS has a much shorter delay in the target/ion source system. This can be seen by comparing the t_{50} values for Sn and SnS. For Sn at a target temperature of 1950°C, the 50% time was determined to be 108 $\pm$ 10 seconds. For SnS, this value reduces to 33.5 $\pm$ 2.5 seconds, corresponding to more than a three-fold reduction in the t_{50} time.

Spejewski, [22] and references therein, has shown that holdup measurements are well fit by a two-exponential function. Accordingly, the fractional build-up curves were fitted with a function of the form

$$F(t) = A(1 - e^{-\lambda_1 t}) + B(1 - e^{-\lambda_2 t}), \tag{2.8}$$

where λ_1 and λ_2 represent the two different time constants for the build-up, and the amplitude coefficients A and B represent the weighting for the two time constants.

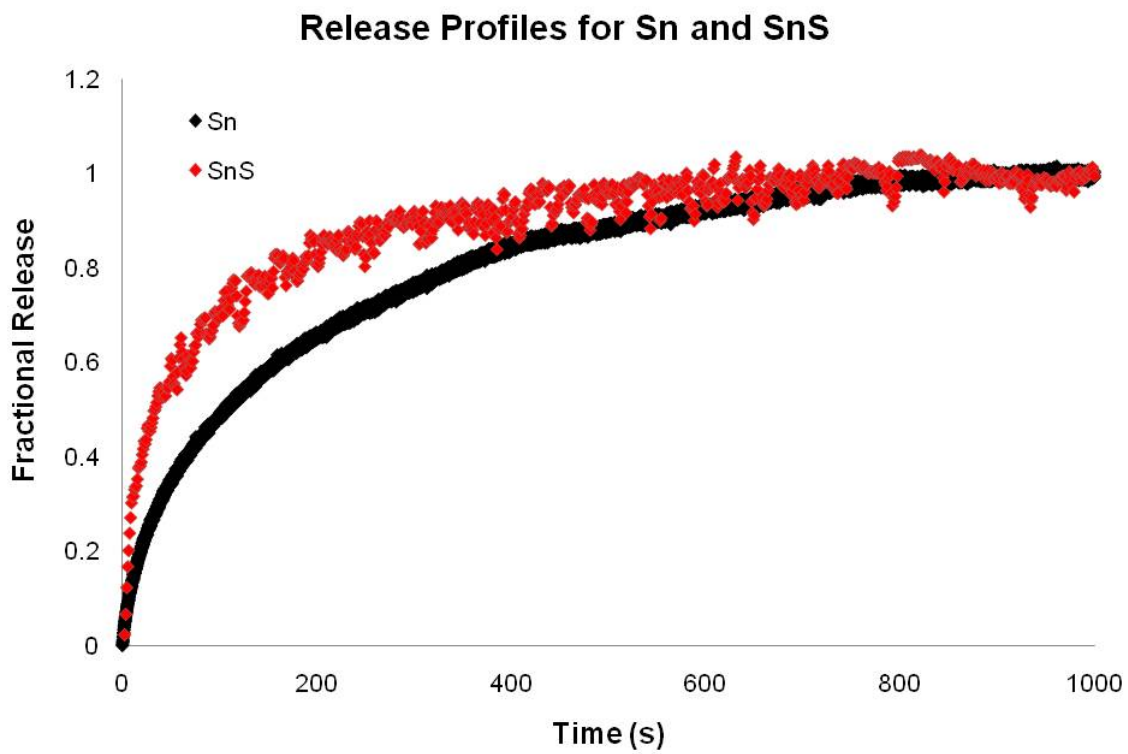

Figure 2.5: Fractional release curves of Sn and SnS measured for a target temperature of 1950 ^{o}C

	t_1	t_2
Sn	25.4 sec (27.4%)	285.7 sec (75.0%)
SnS	15.7 sec (49.1%)	190.5 sec (50.4%)

Figure 2.6: Time constants with associated amplitude coefficients given in parentheses

The time constants can be extracted from the fitting parameters as

$$t_i = \frac{1}{\lambda_i}. \tag{2.9}$$

The fitting was carried out using a Levenberg-Marquadt algorithm for non-linear curve fitting provided in the program Origin [23]. The curves all had statistically good fits, with R^2 values greater than 0.97 and χ^2/DoF$\sim 10^{-5}$.

The time constants and corresponding amplitude coefficients are given in figure 2.6. The short time component for SnS is reduced by almost 40%. The release of Sn as the sulfide is also improved by moving more of the release into the short component. This is seen by comparing the amplitude coefficients for the short time components. About one quarter of the release of Sn is in the short time component, compared to almost half for SnS.

An analysis was performed after fitting the data sets. To calculate the efficiency reduction because of finite half-lives $\epsilon(t_{\frac{1}{2}})$ and the average release time $< t_{release} >$, the release function p(t) was first determined by differentiating the fractional release function. The release function p(t) becomes

$$p(t) = \frac{dF}{dt} = A\lambda_1 e^{-\lambda_1 t} + B\lambda_2 e^{-\lambda_2 t}. \tag{2.10}$$

Inserting this into equations 2.5 and 2.6 and calculating the integrals gives

$$\epsilon(t_{\frac{1}{2}}) = \int_0^\infty p(t)e^{-\lambda t}dt = A\frac{\lambda_1}{\lambda + \lambda_1} + B\frac{\lambda_2}{\lambda + \lambda_2} \tag{2.11}$$

and

$$< t_{release} >= \int_0^\infty t \cdot p(t)dt = (\frac{1}{A+B}) \cdot (\frac{A}{\lambda_1} + \frac{B}{\lambda_2}), \tag{2.12}$$

where the radioactive decay factor in equation 2.11 has been written in terms of the radioactive decay constant λ for convenience. The average release times are calculated as 104.2±2.3 seconds for SnS and 216.0±0.4 seconds for Sn, showing that SnS has a faster release even with its long time component.

Figure 2.7 indicates that the relative efficiency for SnS is less sensitive to half-life reductions, as expected since SnS has a shorter delay time in the TISS. Hence, figures 2.5-2.7 show unambiguously that SnS has a shorter overall delay in the TISS. In other words, the release of SnS is, on average, faster than Sn.

It is not possible, in general, to determine the source of the improved release, as holdup measurements represent an integrated process. It also is not possible, under the current conditions, to determine where the sulfide molecule is formed. Since there is not a substantial difference between the two holdup curves, one reasonable conclusion is that the sulfide is formed primarily within the transfer line and not inside the target holder. Formation of the sulfide molecule in the transfer line would for all intents and purposes reduce the transfer line effusion time to zero because of negligible surface residence times. If this is correct, then the release from the target holder becomes the limiting process for production of radioactive Sn beams. However, it should be possible to reduce the in-target delay time and study the extent to which the transfer line-induced delay affects the release of Sn and SnS. To do this requires modifying the target/ion source system to give improved control over the release properties of atoms and molecules.

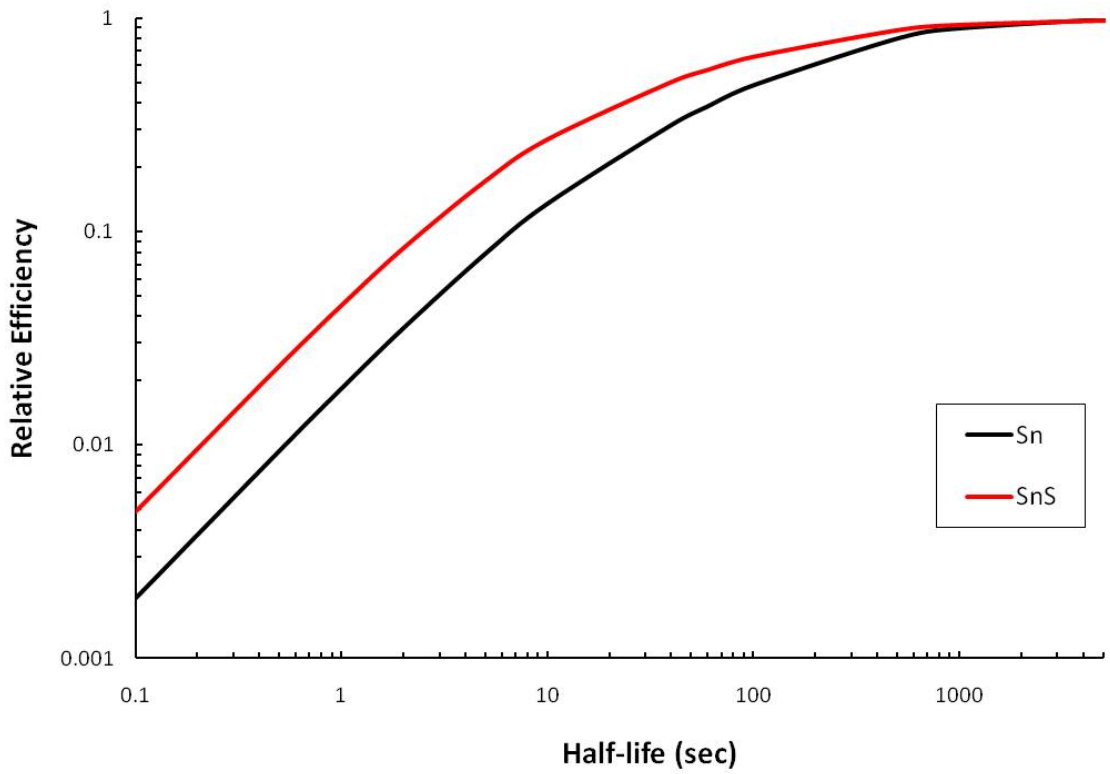

Figure 2.7: Efficiencies for finite half-lives calculated from equation 2.11. The quoted efficiency is relative to the system efficiency measured for a stable beam.

Chapter 3

Modified HRIBF-type Target/Ion Source System

3.1 Design

The standard HRIBF-type target/ion source system was modified to provide greater flexibility in the temperature distribution of the target/ion source system and to minimize the release time of molecules.

A technical drawing of the modified target/ion source system, with the primary components labeled, is provided in figure 3.1. The materials used in the construction of the modified TISS are essentially the same as those used in the construction of the standard TISS, i.e., primarily tantalum and graphite. They were chosen because of their refractory nature. In addition to the tantalum and graphite, one primary component was made from molybdenum. Molybdenum, also refractory, was chosen for the second current strap-separator piece to prevent high-temperature welding of the transfer line and cathode. Under normal operating conditions, i.e. around 2000 ^{o}C, tantalum parts in contact with each other, but not directly welded, almost certainly are subject to a thermal welding. Thus, inserting a molybdenum part to separate the tantalum transfer line and tantalum cathode should prevent thermal

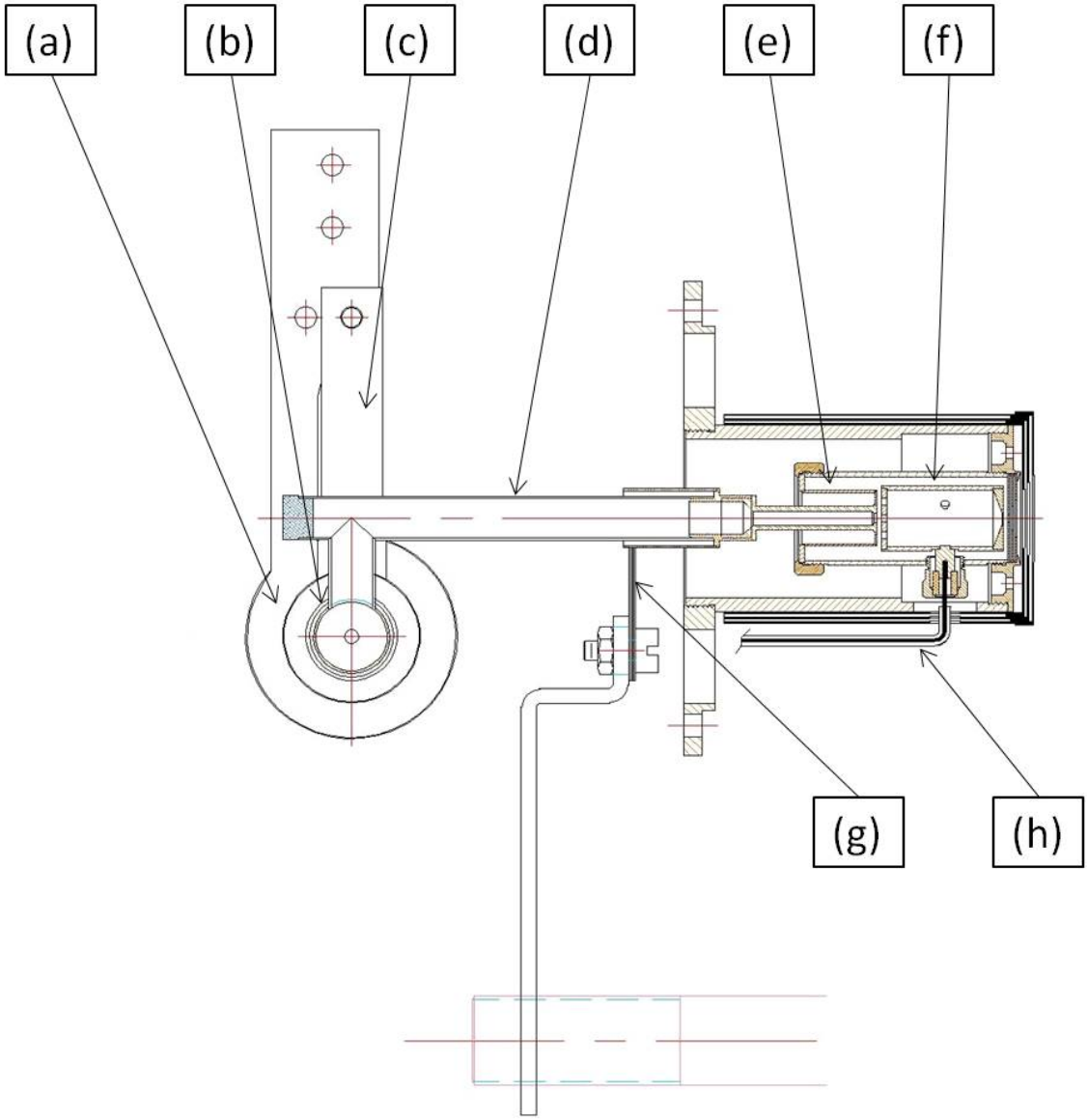

Figure 3.1: Technical drawing of the modified HRIBF-type target/ion source system. Parts labeled are: (a) target heater, (b) target holder, (c) current strap 1, (d) transfer line, (e) cathode, (f) anode chamber, (g) current strap 2 and adaptor, and (h) anode voltage wire

welding, affording greater flexibility in reusing parts. Furthermore, connecting the molybdenum current strap to the separator piece allows the cathode current and transfer line current to flow into or out of the system at the end of the transfer line. This allows the transfer line current to flow along essentially the entire transfer line.

In the standard TISS, the cathode current is driven through a single current strap located at the beginning of the transfer line and thus ohmically heats the transfer line. Unlike the standard TISS, this modified design relies on two current straps to introduce two of the three currents. The target is heated in the usual way, i.e., a large current, nominally around 750 A, is driven through a heater element that surrounds the target holder.

Due to physical limitations of the setup, it was decided to make use of the three existing current feedthroughs to construct the transfer line circuit. This was only possible because the target heater circuit is electrically isolated from the existing cathode circuit. As shown in figure 3.2, the transfer line circuit is completed by sharing two of the existing feedthroughs with the target heater and cathode. Current Strap 1 connects into the negative terminal of the target heater, and Current Strap 2 connects into the feedthrough for the cathode current. In this way, the transfer line current is driven through Current Strap 1, flows along the transfer line, and exits through Current Strap 2. The normal cathode current can still be maintained by driving the cathode current through Current Strap 2 to chassis ground. Thus, an additional current to heat the transfer line is introduced without affecting the existing cathode and target heater circuits.

The originial hypothesis that the molecules are forming on the surface of the transfer line indicated that it may be possible to improve the release efficiency of those molecules by forming the molecule inside the target holder itself. To accomplish this, the gas feed line is inserted into the back of the target holder directly, thus ensuring the molecule-creating gas saturates the surfaces of the target container.

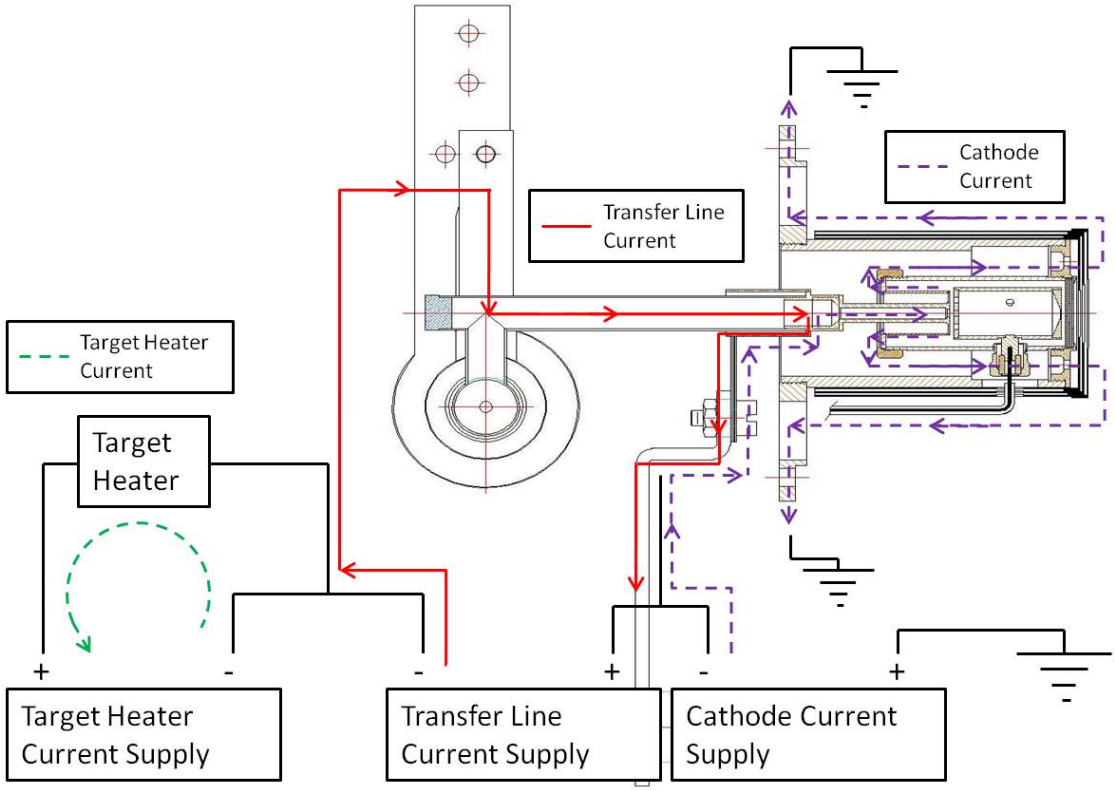

Figure 3.2: Diagram illustrating the electrical circuit for the modified HRIBF-type TISS. The new transfer line current is indicated with a solid line, whereas the previously existing currents are indicated with dashed lines.

3.2 Construction

Photographs of the modified target/ion source system, with several of the main components labeled, are shown in figures 3.3 and 3.4.

The target holder is a simple open-ended tantalum tube measuring 1.32 inches long and having an inner diameter of 0.089 inches. These dimensions limit the size of the target used. The target insert was made from the high-purity Poco AXZ-5Q graphite, with an inner diameter of 0.615 inches and an inner length of about 0.78 inches. The target holder and graphite insert have a small 0.335-inch hole drilled through the top, providing an exit aperture for the reaction products. The transfer line consists of two pieces of tantalum tubing joined to provide a 90° bend in the transfer line. The transfer line is made from tantalum tubing with an outer diameter 0.375 inches and a wall thickness of 0.020 inches. The vertical piece of the transfer line is welded to the target holder, and the two pieces of the transfer line are welded together.

The current strap positioned at the front-most end of the transfer line (labeled as Current Strap 1 in figure 3.1) is constructed from 10 pieces of 0.005 inch thick tantalum sheets, electron welded at the tips. This design allows the strap to be bent more easily than a single piece of 0.05 inch thick tantalum. A solid tantalum rod is used to connect Current Strap 1 to the negative leg of the target heater. This avoids creating a *de facto* cantilever, which would allow the soft tantalum metal to deform and sag at high temperatures. The solid rod provides some support for the target holder, ensuring that the target holder remains aligned with the beam line.

The second current strap (Current Strap 2) and the separator piece were constructed from molybdenum. Molybdenum, with a melting temperature in excess of 2600 ^{o}C, is sufficiently refractory for use in high-temperature target/ion source systems. Furthermore, using molybdenum for the part that separates the transfer line and cathode should prevent high-temperature welding of the transfer line and

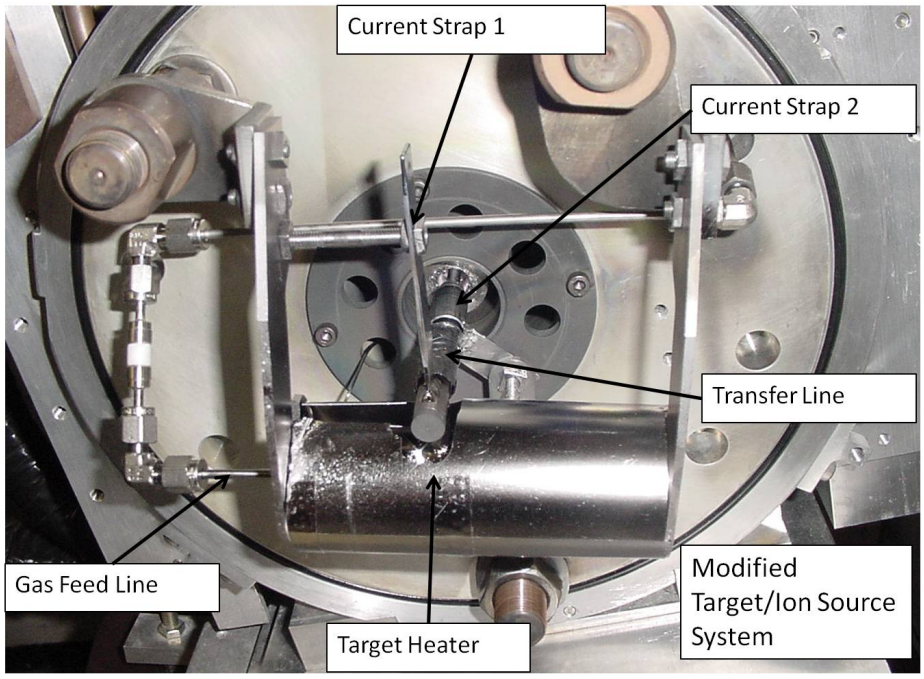

Figure 3.3: Front view of the modified target/ion source with the main components labelled.

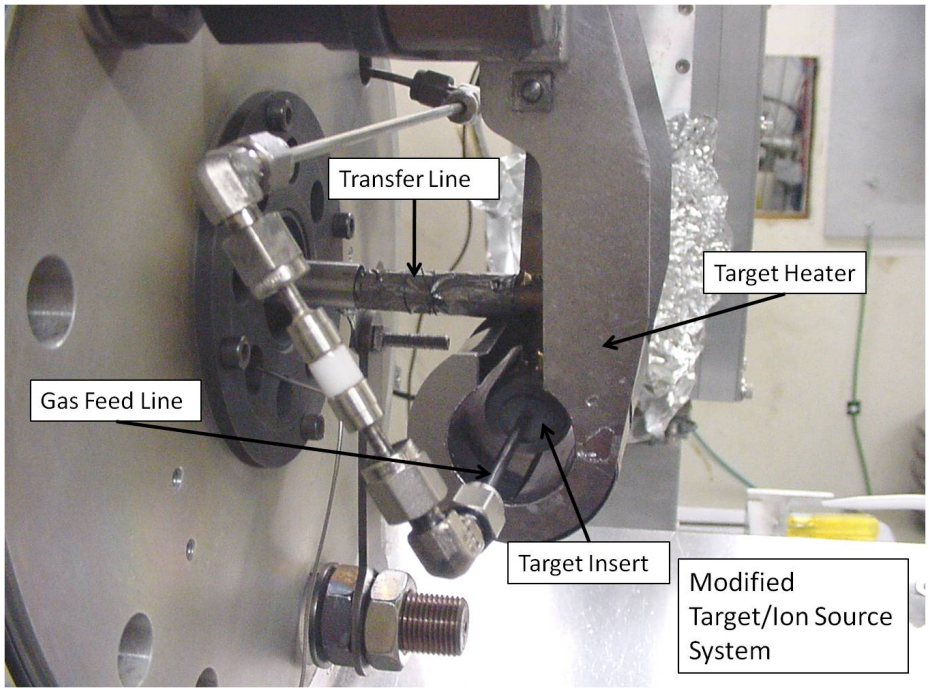

Figure 3.4: Side view showing the gas line and target insert.

cathode. This preventive measure allows for the replacement of defective or worn-out parts. The ability to reuse the cathode-ion source and/or the target-transfer line assembly reduces substantially the assembly time for a single target/ion source system if repairs are needed. The molybdenum separator connects to the transfer line on one side and the cathode on the other side, using a slip-fit connection for both. As with Current Strap 1, Current Strap 2 is constructed from 10 pieces of 0.005 inch thick sheets. However, molybdenum is more brittle than tantalum, so care must be taken to avoid applying an unintended torque to the strap.

The gas feed line consists of three segments. The first segment is a tantalum tube of 0.125 inch outer diameter and a wall thickness of 0.020 inches. The exit aperture of the tantalum tube is reduced to 0.01 inches to minimize the fraction of reaction products that are allowed to migrate into the gas line. Unfortunately, reducing the exit aperture may also reduce the krypton and xenon system efficiencies by decreasing the conductance of the gas line. One end of the tantalum tube is inserted into the back of the graphite target insert, and the other end is connected to an electrical insulator to avoid providing more than one path to chassis ground. The third segment of the gas feed line is made from a stainless steel tube with an outer diameter of 0.125 inches and constitutes the remainder of the gas line.

To minimize the number of modifications to the TISS and thereby limit the number of effects introduced, the HRIBF Electron Beam Plasma ion source is used in this modified TISS. The cathode is adapted from the ISOLDE design described in [24]. The cathode is designed to be a high-resistance piece, allowing for more efficient resistive heating. The cathode interior consists of an open tube to allow reaction products to pass from the transfer line to the anode. The anode is a tantalum chamber with a hexagonal grid facing the cathode and a single aperture near the extractor lens. The grid provides a measure of physical containment, preventing atoms and ions from leaving the anode chamber without being extracted. The anode chamber is isolated electrically from the cathode by means of three Al_2O_3 insulators. Insulating the anode from the cathode allows the anode to be maintained at a positive

potential relative to the cathode, a condition necessary for accelerating the primary electrons used in electron-impact ionization.

3.3 Characterization

Two different parameters were measured to characterize the modifications to the target/ion source system. First, to ensure that the ion source works, the xenon and krypton efficiencies were measured. Measuring the efficiencies for krypton and xenon demonstrates unambiguously that feeding the gas line into the target insert allows gases to flow through the entire target/ion source system. This method also gives a more accurate representation of the system delay and system efficiency for gases than is available using the standard design.

The maximum currents for ^{84}Kr and ^{132}Xe were measured to be 53.6 nA and 14.9 nA, respectively. Using the conversion of 1.6 nA$\approx 1 \cdot 10^{10}$ ions/sec, the total system efficiencies were determined to be about 5.9% for krypton and 3.9% for xenon. These low efficiencies likely result either from the reduced apertures of the individual pieces of the gas line [25], or from an inefficient ion source. However, measured beams of ever-present contaminants, such as mass 35 (^{35}Cl) and mass 28 (probably from N_2 seeping into the vacuum chamber through known minor vacuum leaks in the system), would seem to indicate the ion source was operating efficiently.

The second parameter measured was the temperature distribution of the TISS, which was characterized by measuring the temperature of the target and the temperature of the transfer line. Measurements were taken for several target and transfer line currents.

Temperature measurements were made using a single-color optical pyrometer, calibrated by ORNL's metrology department. Optical pyrometers work on the principle of color matching. The pyrometer contains a thin filament that can be heated by an adjustable current. The temperature of the object is measured by adjusting the current flowing through the filament until the color of the filament matches the

color of the object. The (uncorrected) temperature is then read directly from the pyrometer's gauge. The optical pyrometer assumes the object is a perfect blackbody, so that a correction factor must be applied to account for thermal emmissivities less than one. A temperature-dependent correction factor is then applied to the measured temperature to determine the actual temperature of the object.

The transfer line temperature was measured at two points along the transfer line, labelled as 'Position 1' and 'Position 2' in figure 3.5. These points correspond approximately to the beginning of the transfer line and the middle of the transfer line. More points of measure were not possible because the transfer line contains heat shielding, which is necessary to minimize losses from thermal radiation. Between the two points of measurement, the transfer line is wrapped twice in a thin sheet of Ta foil that is crumpled to reduce physical contact. The transfer line beyond Position 2 is obscured from view by the molybdenum tube. The molybdenum tube should also act as a heat shield, thereby protecting that portion of the transfer line from becoming a cold spot.

The variability of the target temperature was determined by measuring the temperature of the target insert for several target heater currents, ranging from 300 amps to 800 amps. Figure 3.6 shows that the target temperature can be varied over a dynamic range of more than 800 ^{o}C with the existing current supply.

The measured temperature distribution of the transfer line corresponding to different target temperatures is shown in figures 3.7 and 3.8. The plots show that there is a marked difference in the temperature profiles between positions 1 and 2. This is believed to be a result of heat dissipation at Position 1. Heat shields were not applied there so that the temperature could be measured more easily. This will be changed in future target/ion source systems, allowing for a more even temperature distribution along the transfer line.

A transfer line current of 450 A is not the maximum current that can be driven. The power supply being used is a high-current, low-voltage supply with a voltage limit of 8.5 V. A transfer line current of 450 A corresponds to a voltage drop of about

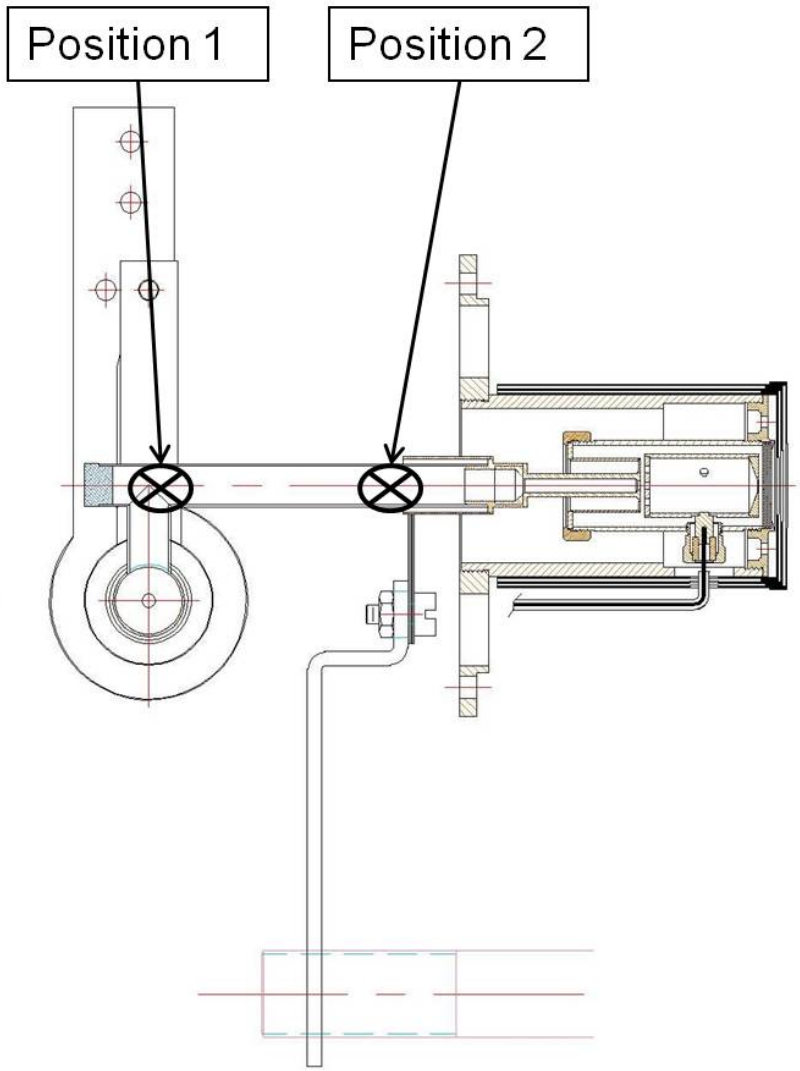

Figure 3.5: The two points at which the transfer line temperature was measured.

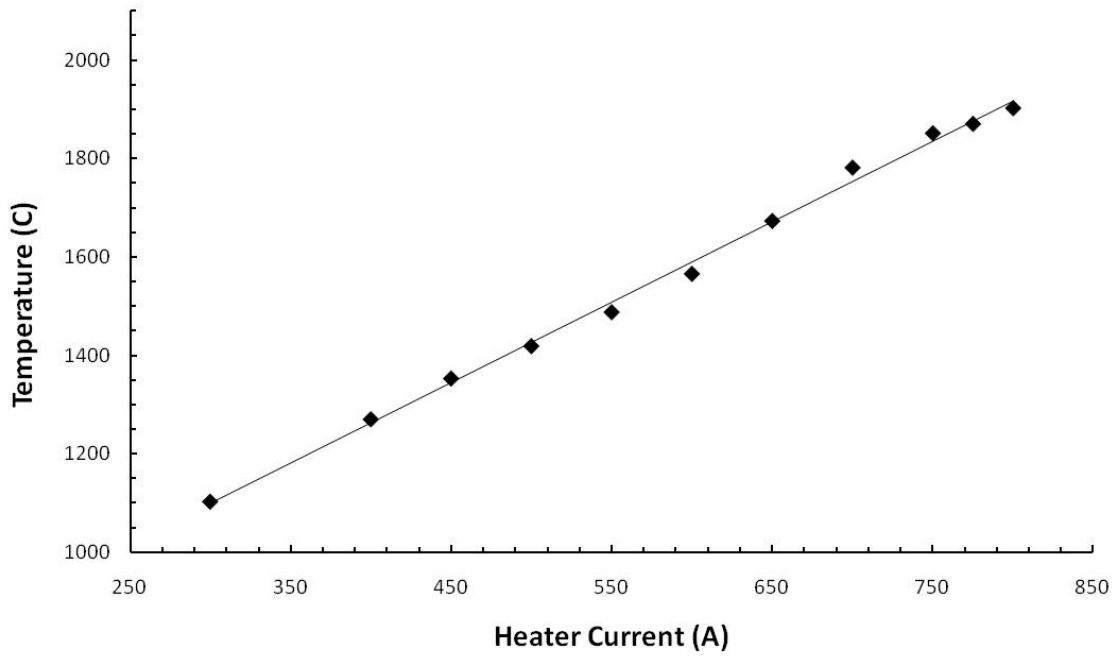

Figure 3.6: Temperature of the target as determined by measuring the temperature of the graphite insert.

5.4 volts. The voltage limit imposed by the supply allows for a maximum transfer line current greater than 550 A.

Extrapolating to 550 A on the transfer line and at the highest target temperature, figure 3.9 shows that it should be possible to achieve a transfer line temperature in the range of about 2100 ^{o}C to 2300 ^{o}C. The less impressive temperature at Position 1 indicates that heat losses from thermal radiation are beginning to dominate the heating process, indicating that higher temperatures are not possible unless additional heat shielding is applied. Applying improved heat shielding should then allow access to transfer line temperatures in the range of 2300 ^{o}C.

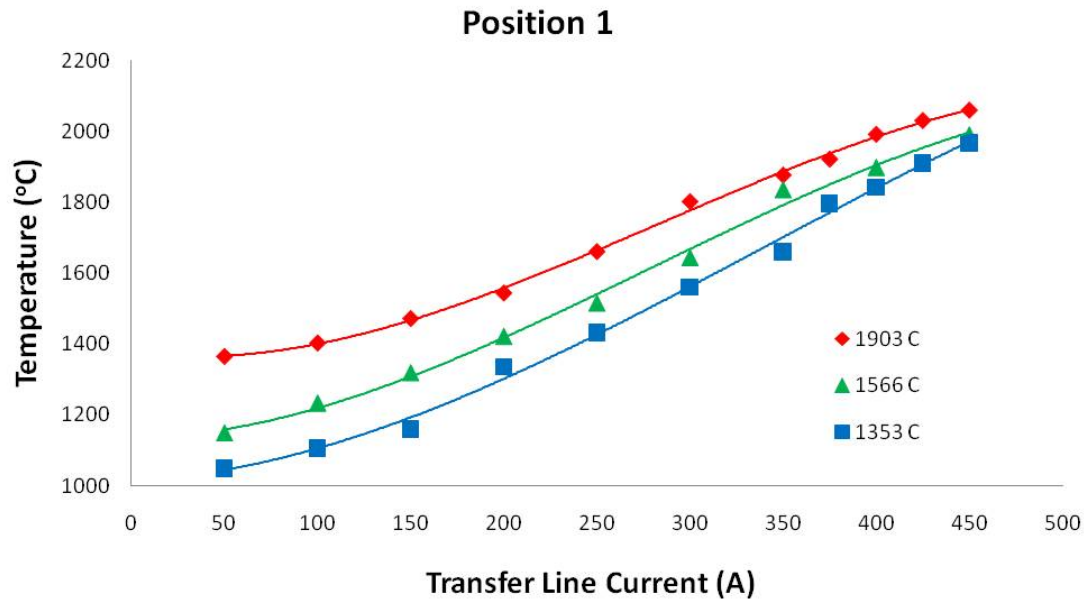

Figure 3.7: Transfer line temperature as a function of applied current measured at Position 1. The three plots correspond to the three different target temperatures for which the transfer line temperature was measured.

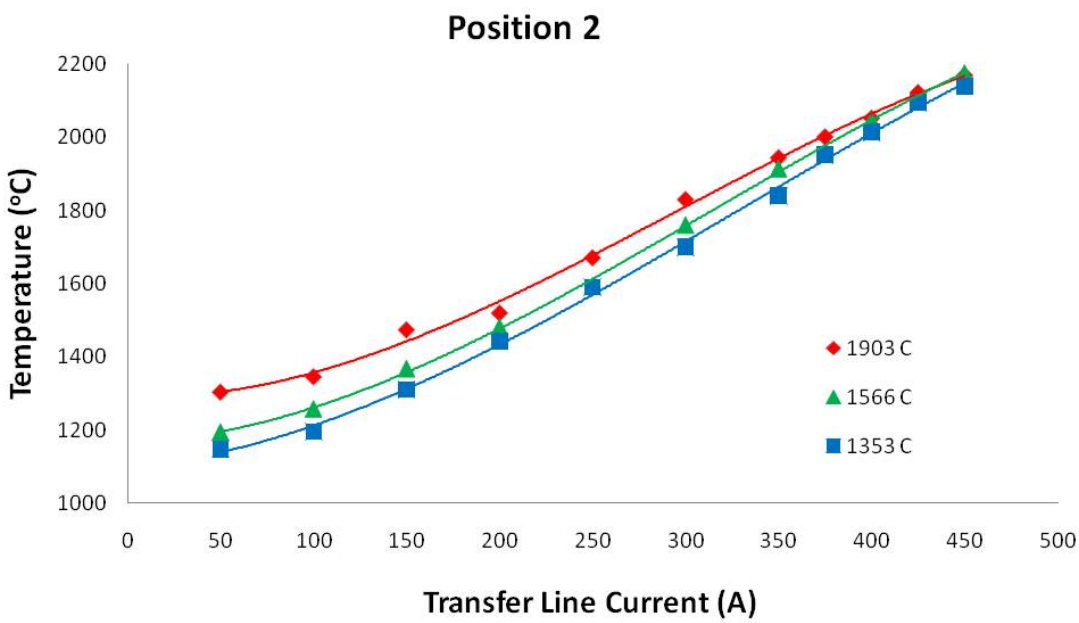

Figure 3.8: Transfer line temperature as a function of applied current measured at Position 2. The three plots correspond to the three different target temperatures for which the transfer line temperature was measured.

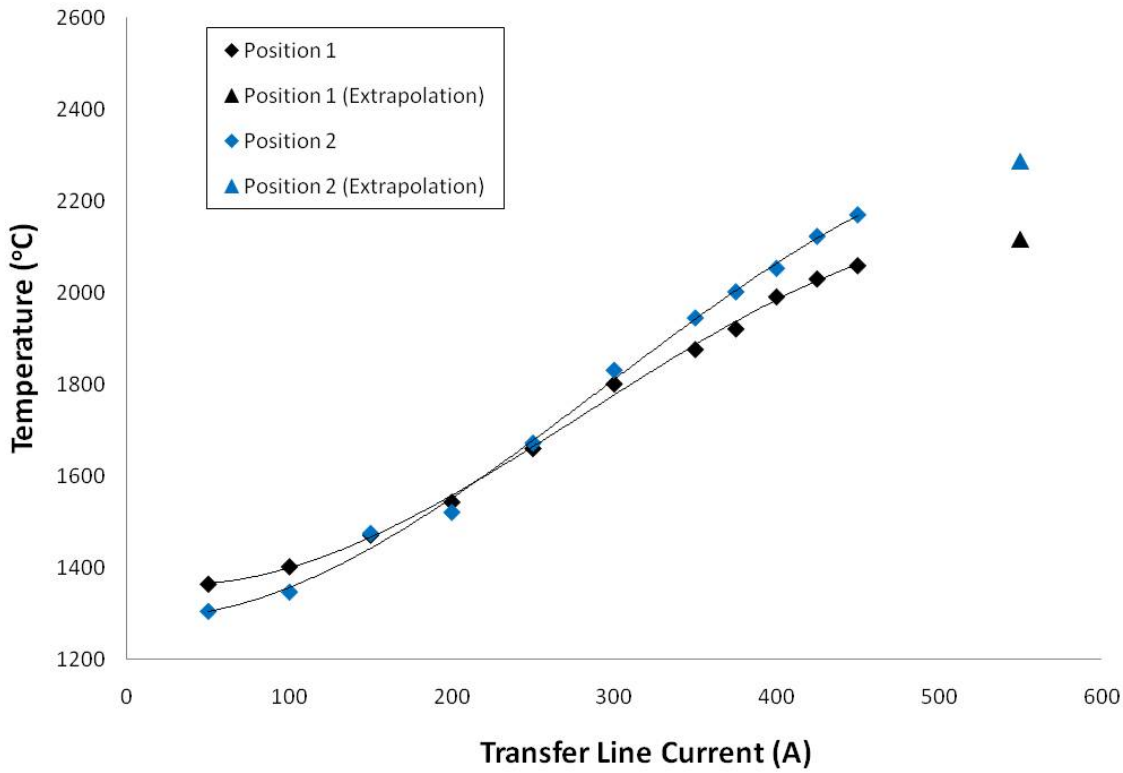

Figure 3.9: Transfer line temperature distributions for a target temperature of 1900 ^{o}C showing the temperatures extrapolated to a transfer line current of 550 A.

Chapter 4

Conclusions and Implications for Future Research

Extraction of Sn isotopes in the sulfide molecular sideband has been shown to reduce the delay time of Sn atoms inside a target/ion source system. It has also been shown to reduce the isobaric contamination by moving the Sn isotopes to a mass region that does not contain significant radioactivity. Both of these effects improve the quality of radioactive Sn beams available for study.

A preliminary experiment was carried out to measure the delay of Sn and SnS in the TISS used at the HRIBF. The measurement of the holdup of SnS was the first measurement of its kind for the HRIBF system. The results obtained from this measurement confirm that SnS has a shorter overall delay in the system. Analysis of the data, in conjunction with the results obtained by Kirchner, indicates that improvements in the formation and release of SnS are possible.

Unfortunately, the target/ion source design currently employed at the HRIBF does not afford enough flexibility to investigate and optimize the release of Sn isotopes in the sulfide sideband. A modified TISS was designed, built, and tested. The modified design allows for independent and controlled heating of the transfer line and feeds the molecule-creating gas directly into the target holder, thereby ensuring that the gas

coats the surfaces of the target and transfer line. Results from the characterization measurements show that the target can be heated to temperatures in the range of 1100 ^{o}C to 1900 ^{o}C. The transfer line circuit incorporated into this new design represents a significant improvement over earlier designs because the transfer line can now be heated to temperatures ranging from about 1000°C to more than 2100 ^{o}C. The system efficiency was measured to be between 3% to 5% for krypton and xenon.

The standard HRIBF target/ion source system is not capable of independently heating the transfer line. As designed, the transfer line is heated by forcing the cathode current (typically around 350 amps) to flow along the transfer line. According to figures 3.7 and 3.8, 350 amps of current flowing along the transfer line corresponds to transfer line temperatures between 1875-1950 ^{o}C, depending on the position and amount of heat shielding used. The lowest temperature is customarily used for characterization, as the colder parts of the transfer line will dominate the effusion time. Thus, the standard TISS operates with a transfer line temperature of approximately 1875 ^{o}C. Using Kirchner's ΔH_{ads} value of 4.5 eV for Sn on a tantalum surface [9], this corresponds to a sticking time of 87 μs. However, the sticking time for Sn can be reduced to 14 μs, a 6-fold reduction, simply by increasing the transfer line temperature to about 2050 ^{o}C. If, however, the transfer line temperature is increased to 2300 ^{o}C, then the sticking time is reduced further to about 1.6 μs.

As mentioned in section 1.3.1, a critical parameter in optimizing the formation of SnS molecules is the ratio of $\frac{t_f}{t_s}$, where t_s is the sticking time and t_f is the mean formation time. The formation probability for creating SnS increases asymptotically as t_s becomes much larger than t_f. A quick calculation shows that for a temperature of 1300 ^{o}C on the transfer line, Sn has an adsorption time of about 628 ms, otherwise prohibitively long. At this temperature the probability is essentially a maximum. Once formed, though, SnS will be relatively unaffected by the low transfer line temperature. The ΔH_{ads}, deduced from [21], is taken to be approximately 3.38 eV for SnS on a tantalum surface. With this adsorption enthalpy, the sticking time at 1300 ^{o}C is calculated to be about 162 μs, which should not be prohibitively long. If,

instead, the temperature of the transfer line is maintained at about 1600 ^{o}C, then the probability is still sufficiently high at $\beta = 0.75 \cdot \beta_{max}$. At this temperature, the surface residence time for SnS is reduced to about 3 μs. It should be possible, then, to increase the fraction of Sn atoms converted into SnS and to do so earlier in the release process.

Once implemented, the modified target/ion source is expected to improve the release efficiency of Sn, both in its atomic form and as a sulfide. Additionally, the modifications are applicable to molecular sidebands other than the sulfide sideband. On-line measurements are needed, but it is anticipated that the modified target/ion source design will improve the effectiveness of the molecular-sideband technique at the HRIBF. Beyond improvements to the molecular-ion technique, the ability to heat or cool the transfer line is expected to improve the quality of other atomic beams. Increasing the transfer line temperature will reduce the surface adsorption time, thereby improving the release efficiency for the more refractory elements.

Future measurements using the modified target/ion source system will focus on mapping out the release properties of Sn as a function of target and transfer line temperatures, optimizing the formation probability for SnS and, once optimized, measuring the release properties of SnS for the different target and transfer line temperatures. Once the on-line release of Sn in the sulfide sideband has been fully investigated, the yields of neutron-rich Sn isotopes produced in the 40 MeV proton-induced fission of uranium-238 will be measured to demonstrate the improved beam rates made possible by the modifications. Additional measurements will be carried out to determine the extent to which beams of the more refractory elements can be produced.

Bibliography

Bibliography

[1] C. Kittel, *Introduction to Solid State Physics*, John Wiley and Sons, Inc., 7th edition, 1996. 6, 8

[2] M. Fujioka and Y. Arai, Nucl. Instr. and Meth. **186**, 409 (1981). 6

[3] R. Present, editor, *Kinetic Theory of Gases*, McGraw-Hill Book Company, Inc., 1958. 8

[4] A. Zangwill, *Physics at Surfaces*, Cambridge University Press, 1988. 8

[5] M. Knudsen, *The Kinetic Theory of Gases: Some Modern Aspects*, 'John Wiley Sons, Inc.', 3rd edition, 1950. 9

[6] B. Wolfe, editor, *Handbook of Ion Sources*, CRC Press, 1995. 10, 11

[7] K. Jones et al., Nature **465**, 454 (2010). 12

[8] M. Karny et al., Eur. Phys. J. A **25**, 135 (2005). 12

[9] R. Kirchner, Nucl. Instr. and Meth. B **26**, 204 (1987). 12, 16, 47

[10] A. Kronenberg et al., Nucl. Instr. and Meth. B **266**, 4252 (2008). 12

[11] R. Kirchner, Nucl. Instr. and Meth. B **126**, 135 (1997). 12

[12] P. Hoff et al., Nucl. Instr. and Meth. **172**, 413 (1980). 12

[13] P. Hoff, O. Jonsson, E. Kugler, and H. Ravn, Nucl. Instr. and Meth. in Phys. Res. **221**, 313 (1984). 12

[14] D. Stracener, Nucl. Instr. and Meth. B **204**, 42 (2003). 13

[15] R. Kirchner, Nucl. Instr. and Meth. B **70**, 186 (1992). 17, 21

[16] J. Batchelder, 2009, Personal Communication. 25

[17] F. Cowlard, J. Mater. Sci. **2** (1967). 25

[18] J. F. Ziegler, Srim-2010, http://www.srim.org/. 26

[19] National nuclear data center, http://www.nndc.bnl.gov/. 26

[20] D. Stracener, 2008, Personal Communication. 28

[21] R. Kirchner, Nucl. Instr. and Meth. B **204**, 179 (2003). 28, 47

[22] E. Spejewski, Nucl. Instr. and Meth. B **266**, 4271 (2008). 28

[23] OriginLab, Origin, v7.5. 30

[24] S. Sundell, H. Ravn, and the ISOLDE Collaboration, Nucl. Instr. and Meth. in Phys. Res. B **70**, 160 (1992). 39

[25] H. Carter et al., Nucl. Instr. and Meth. B **126**, 166 (1997). 40

Appendices

Appendix A

Derivation of Yield Measurements

The rate of ions/sec of a particular nuclide produced and extracted from the separator is commonly referred to as the yield, Y. This rate can be measured in a relatively straightforward way. To do this, the system is brought to equilibrium, i.e., the difference between the ions/sec extracted from the target/ion source system and the production rate is constant.

To determine the yield of a given nuclide, a moveable tape collector, a detector, and a data acquisition system are employed to measure the activity of the nuclide X. At the end of the collection time interval t_{coll}, the buildup of radioactivity on the tape is

$$N(t_{coll}) = \frac{Y}{\lambda}[1 - exp(-\lambda t_{coll})] \tag{A.1}$$

where λ is the radioactive decay constant. At the end of the collection, the tape is moved in front of the HPGe detector to measure the activity. By the time the collected sample reaches a position in front of the detector, the amount is now

$$N_1(t_m) = N(t_{coll})exp(-\lambda t_m) = \frac{Y}{\lambda}[1 - exp(-\lambda t_{coll})]exp(-\lambda t_m) \tag{A.2}$$

where t_m is the time it takes for the tape to move the collected sample from the point of deposition to a point in front of the detector. When necessary, a delay time t_d

is introduced between the end of the tape move and the start of the counting. This is occasionally necessary when the activity of the sample is sufficiently large as to overwhelm the detector/data acquisition system. Thus, at the start of the counting, the collected sample has been reduced to

$$N_1(t_m + t_d) = \frac{Y}{\lambda}[1 - exp(-\lambda t_{coll})]exp(-\lambda t_m) * exp(-\lambda t_d) \tag{A.3}$$

The sample is counted for a total time t_{count}. The total number of decays occurring during the counting time is given by

$$N_{decay} = \int_0^{t_{count}} \lambda N_1(t)dt \tag{A.4}$$

and is related to the number of γ-rays measured for the transition i by

$$N_\gamma = b_\gamma \cdot \epsilon(E_\gamma) \cdot N_{decay} \tag{A.5}$$

where b_γ is the branching ratio for a given transition, and $\epsilon(E_\gamma)$ is the detector efficiency for measuring a γ-ray of energy E. Thus,

$$N_\gamma = b_\gamma \cdot \epsilon(E_\gamma)\frac{Y}{\lambda}[1 - exp(-\lambda t_{coll})]exp(-\lambda(t_m + t_d))[1 - exp(-\lambda t_{count})] \tag{A.6}$$

Solving for the yield,

$$Y = \frac{N_\gamma \lambda}{b_\gamma \cdot \epsilon(E_\gamma)[1 - exp(-\lambda t_{coll})]exp(-\lambda(t_m + t_d))[1 - exp(-\lambda t_{count})]} \tag{A.7}$$

for a single cycle. Often, though, several cycles of collecting/counting need to be performed to build up a sufficient number of counts to minimize the statistical errors in N_γ. Thus, the yield Y' becomes $Y' = Y/n$, where n is the number of cycles.

Appendix B

Adsorption Times

Figures B.1-B.3 show plots of the calculated surface adsorption time for enthalpies of adsorption ranging from 1-6 eV at the different surface temperatures indicated. These plots illustrate the sensitivity in surface sticking times, particularly for the more refractory elements (ΔH_{ads} greater than about 5 eV), for different surface temperatures. The surface temperature of 1875 ^{o}C corresponds to the temperature of the transfer line in the standard HRIBF target/ion source system. The temperature dependence of the surface residence time is shown for Sn and SnS in figure B.4, where the enthalpies of adsorption are taken from Kirchner's work.

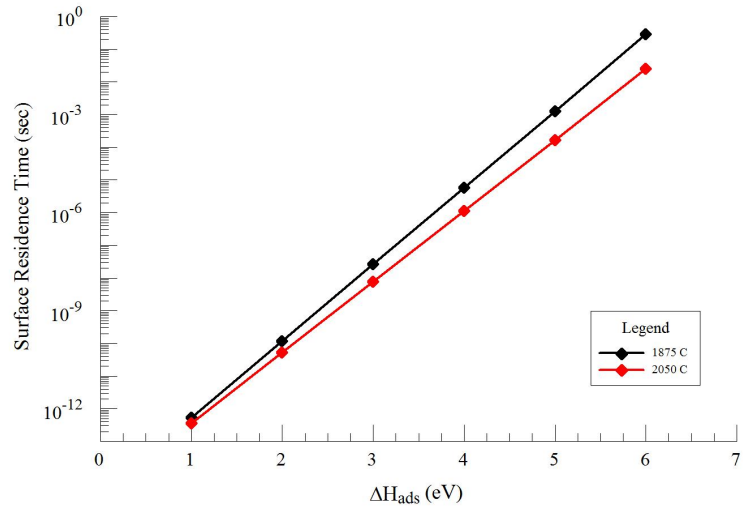

Figure B.1: Adsorption times for surface temperatures of 1875 ^{o}C and 2050 ^{o}.

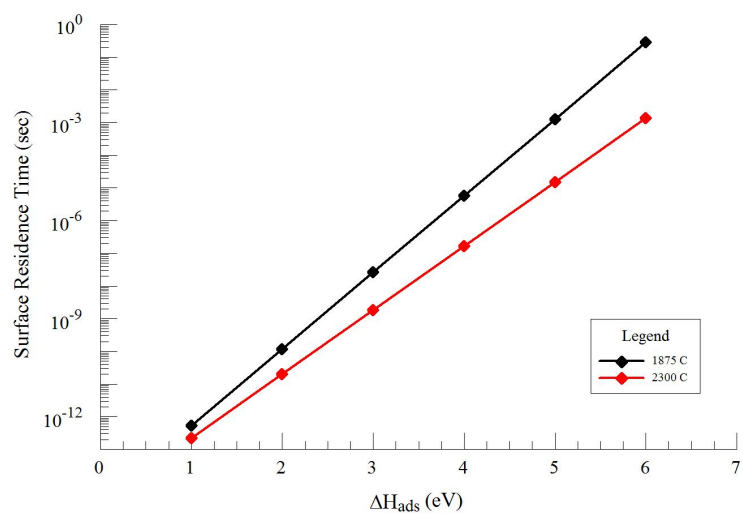

Figure B.2: Adsorption times for surface temperatures of 1875 ^{o}C and 2300 ^{o}.

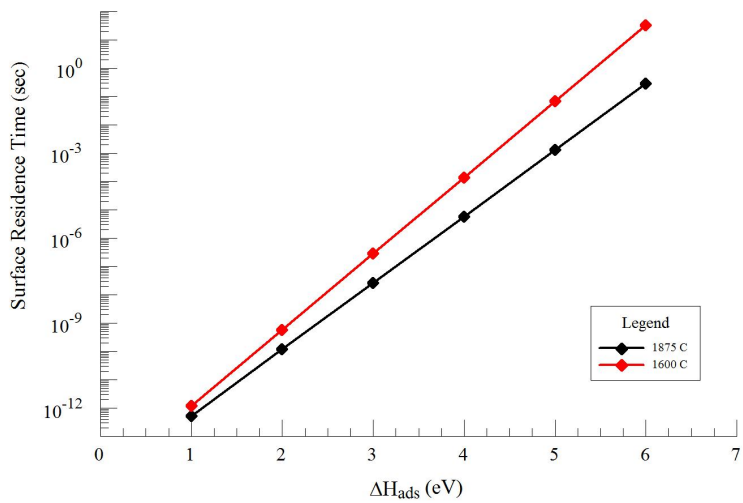

Figure B.3: Adsorption times for surface temperatures of 1875 ^{o}C and 1300 ^{o}.

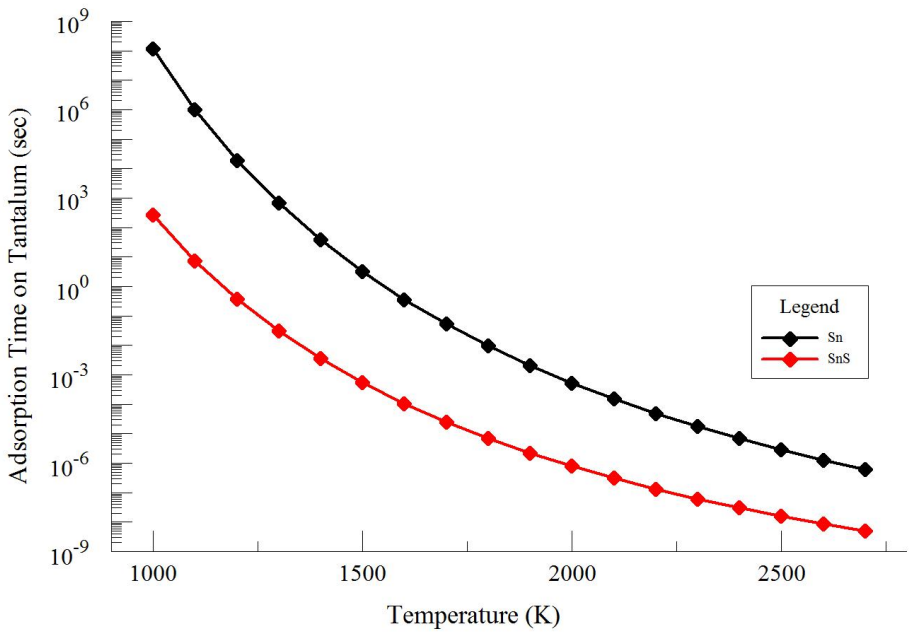

Figure B.4: Plot of the sticking time (per wall collision) as a function of temperature for Sn and SnS adsorbing to a tantalum surface. The values for the enthalpies of adsorption are taken from [9] and [21].

Vita

Ronald Earl Goans was born in Waldorf, Maryland, to parents Ronald Earl Goans Sr. and Judy Winegar Goans. After graduating from Clinton High School in Clinton, TN in 2003, Ronald attended the University of Tennessee at Knoxville. He graduated in August 2007 with a Bachelor of Science degree in Physics. He began graduate studies at the University of Tennessee at Knoxville the following academic year. In subsequent years, he has held a Graduate Teaching Assistantship and a Graduate Research Assistantship. His thesis research was funded by the Center of Excellence for Radioactive Ion Beam Studies and Stewardship Science and was conducted at the Holifield Radioactive Ion Beam Facility at Oak Ridge National Laboratory. Ronald will graduate with a Master of Science degree in Nuclear Physics in May 2011.